Statistical analysis of the long-range transport of the 2015 Calbuco volcanic eruption from ground-based and space-borne observations

Nelson Bègue[1], Lerato Shikwambana[2,3], Hassan Bencherif[1,3], Juan Pallotta[4], Venkataraman Sivakumar[3], Elian Wolfram[4], Nkanyiso Mbatha[5], Facundo Orte[4], David Jean Du Preez[1,6], Marion Ranaivombola[1], Stuart Piketh[7] and Paola Formenti[8]

[1] Laboratoire de l'Atmosphère et des Cyclones, UMR 8105 CNRS, Université de la Réunion, Reunion Island, France.

[2] Space science Division, South African National Space Agency, Hermanus 7200, South Africa

[3] School of Chemistry and Physics, University of KwaZulu-Natal, Private Bag X54001, Durban 4000, South Africa

[4] Centro de Investigaciones en Láseres y Aplicaciones, UNIDEF (CITEDEF-CONICET), 5 Villa Martelli, B1603ALO, Buenos Aires, Argentina

[5] University of Zululand, Department of Geography, KwaDlangezwa, 3886, South Africa

[6] Department Geography, Geoinformatics and Meteorology, University of Pretoria, Pretoria, 0002, South Africa

[7] North-West University, Potchefstroom, South Africa

[8] Laboratoire Interuniversitaire des Systèmes Atmosphériques, UMR CNRS 7583, Université Paris-Est-Créteil, Université de Paris, Institut Pierre Simon Laplace, Créteil, France

Correspondence to: N.Bègue (nelson.begue@univ-reunion.fr)

Abstract

This study investigates the influence of the 2015 Calbuco eruption (41.2°S, 72.4°W; Chile) on the total columnar aerosol optical properties over the Southern Hemisphere. The well-known technic of sunphotometry was applied for investigation of the transport and the spatio-temporal evolution of the optical properties of the volcanic plume. The CIMEL sunphotometer measurements performed at 6 South American and 3 African sites were statistically analyzed. This study involves the use of the satellite observations and a back-trajectory model. The passage of the Calbuco plume is statistically detectable on the aerosol optical depth (AOD)

observations obtained from sunphotometers and MODIS. This statistical detection confirms that the majority of the plume was transported over the northeastern parts of South America and reached the South African region one week following the eruption. The plume has impacted to a lesser extent the southern parts of South America. The highest AOD anomalies were observed over the northeastern parts of the South America. Over the South African sites, the AOD anomalies induced by the spread of the plume were quite homogeneously distributed between the east and west coast. The optical characteristics of the plume near source region was consistent with a bearing-ash plume. Conversely, the remote sites to the Calbuco volcano were influenced by ash-free plume. The optical properties discuss on this paper will be used as inputs for numerical models for further investigation on the ageing of the Calbuco plume in a forthcoming study.

1. Introduction

Given that the major volcanic eruptions have the potential to inject large amounts of sulfur into the stratosphere, they are considered as one of the main sources of stratospheric sulfur (Carn et al., 2015; Thomason et al., 2007). Sulphate aerosols are formed in the volcanic plume by aqueous and gaseous oxidation of sulfur dioxide (SO_2) and the subsequent nucleation and accumulation of particles and droplets (Watson and Oppenheimer, 2000). Volcanic emissions may have a significant impact on the atmospheric composition and radiative budget (McCormick et al., 1995; Solomon et al., 1999, 2011). McCormick et al. (1995) showed that following a major volcanic eruption the increase aerosols loading can lead to significant warming of the middle atmosphere. For instance, a warming ranging from 1°C to 4°C was observed in the tropical stratosphere following the Pinatubo eruption in 1991 (Labitzke and McCormick et al., 1992; Young et al., 1994). Through the use of ground-based and satellite observations, various studies have shown that a significant ozone loss occurs following a major volcanic eruption (Hofmann and Oltmans, 1993; Solomon et al., 2005). The sulphate aerosols formed following these events provide surfaces for heterogeneous chemical reactions, which lead to ozone depletion (Tie and Brasseur, 1995; Solomon et al., 1996; Bekki et al., 1997).
Previous studies have also pointed out that moderate volcanic eruptions (i.e, volcanic explosive index between 3 and 5) can significantly modulate the stratospheric aerosol loading compared to the “background period” (i.e, free from the effects of a major volcanic eruption) (Haywood et al., 2010; Neely III et al., 2013). Both ground-based (Hofmann et al., 2009; Trickl et al., 2013; Zuev et al., 2017) and satellite (Vanhellemont et al., 2010; Vernier et al., 2011) observations suggest that the aerosol optical depth (AOD) of the stratospheric aerosol layer

between 20 and 30 km has increased by 4 - 10% per year since 2000. Through the use of the Whole Atmosphere Community Climate Model (WACCM version 3), Neely III et al. (2013) showed that the increase in AOD of the stratospheric aerosol layer is likely due to moderate volcanic eruptions. Satellite observations confirm that the decadal increase in stratospheric aerosol loadings are linked to a series of moderate volcanic eruptions that each injected around a megaton of SO_2 in the lower stratosphere (Vernier et al., 2011). In spite of the fact that these recurrent volcanic eruptions inject less SO_2 than major volcanic eruptions, they can impact the atmospheric radiation budget. Furthermore, taking into account the stratospheric aerosol burden in climate models has been shown to be necessary since their trend has led to a significant counterbalance of the global warming, so called the global warming hiatus (Solomon et al., 2011; Fyfe et al., 2013; Haywood et al., 2013; Ridley et al., 2014; Santer et al., 2014). The use of the Canadian Earth System Model (CanESM2), Fyfe et al. (2013) revealed that the moderate volcanic activity since 2000 has contributed to a reduction of global warming with an impact of -0.07 ± 0.07 K. Based on the use of the coupled atmosphere ocean Earth System model (HadGEM2-ES), Haywood et al. (2013) showed a global mean cooling around -0.02 to -0.03 K over the period 2008-2012 period**.** They showed that the eruptions may result the perceived hiatus in global temperatures caused by the small cooling effect but do not appear to be the primary cause. These previous studies highlight the importance of the stratospheric aerosol burden in climate models and to pursue the analysis of the moderate volcanic activity.

The moderate volcanic eruptions are considered as the most influential events on the stratospheric aerosol burden during the last decade. These moderate volcanic eruptions have mainly been observed in the Northern Hemisphere (Bourassa et al., 2010; Clarisse et al., 2012; Jégou et al., 2013; Kravitz et al. 2010; Sawamura et al., 2012). The Southern Hemisphere was mainly affected by three moderate eruptions since 2010: (1) the Puyehue-Cordon Caulle (40.3°S, 72.1°W; Chile) in June 2011 which emitted 0.2 Tg of SO_2 into the upper troposphere and lower stratosphere (UTLS); Clarisse et al., 2013; Theys et al., 2013; Koffman et al., 2017), (2) the Kelut eruption (7.5°S, 112.2°E; Indonesia) in Feburary 2014, which injected 0.1-0.2 Tg of SO_2 into the stratosphere (Kristiansen et al., 2015; Vernier et al., 2016), and (3) the Calbuco eruption (41.2°S, 72.4°W) in April 2015 which released 0.2 - 0.4 Tg into the UTLS (Bègue et al., 2017; Reckziegel et al., 2016; Mills et al., 2016). The amounts of SO_2 injected during these events are smaller than those injected during the moderate eruptions which occurred in the Northern Hemisphere. For instance, the estimation of SO_2 reported for these three moderate eruptions are 10 - 20 times smaller than the Nabro (13.4°N, 41.7°E; Eritrea) in June 2011 (Bourassa et al., 2012; Sawamura et al; 2012), and a quarter of the amount emitted by the

Sarychev (48.1°N, 153.2°E; the Kuril Islands) in June 2009 (Clarisse et al., 2012; Kravitz et al., 2011; Jégou et al., 2013). This present study focuses on the analysis of the Calbuco eruption. After 43 years of inactivity, the Calbuco volcano in Chile erupted on the 22 April 2015 followed by two intense explosive events recorded during the same week. The volcanic plume spread extensively in the Southern Hemisphere, explained by the dynamical context (Bègue et al., 2017). Through the analysis of advected Potential Vorticity fields derived for 400 K isentropic level from MIMOSA (Modèle Isentropique de transport Mésoéchelle de transport de l'Ozone Stratospherique par Advection) and the Dynamical BArrier Location model (DyBAL; Portafaix et al., 2003), Bègue et al. (2017) showed that volcanic aerosols are predominantly transported eastward in planetary-scale tongues. The transport of the volcanic aerosol plume was modulated by the location of the subtropical barrier and polar vortex, within which most of the zonal transport took place during the first week following the eruption (Bègue et al., 2017). During the same year, the Antarctic ozone hole reached a historical record daily average size in October. The influence of the Calbuco eruption on this significant Antarctic ozone depletion has been debated. Through the use of Specified Dynamics–Whole Atmosphere Community Climate Model (SD-WACCM) and balloon observations at Syowa (69.1°S, 34.6° E), Solomon et al. (2016) found that the Calbuco eruption might be responsible for the extreme ozone depletion recorded over Antarctic during October 2015. Using the WACCM model in its free-running configuration, previous works reveal a significant Antarctic ozone column losses following the moderate Calbuco eruption (Solomon et al., 2016; Ivy et al., 2017). Based on the use of WACCM model and balloon observations at Syowa, South Pole and Neumayer (70.4°S, 8.2°W), Stone et al. (2017) confirmed the assumption that enhanced ozone depletion was mainly due to the Calbuco aerosols. Particularly, these stratospheric volcanic aerosols greatly enhanced austral ozone depletion at 100 - 150 hPa between 55°S and 68°S (Stone et al., 2017). More recently, Zhu et al. (2018) showed that the Calbuco aerosols depleted around 25% of ozone near 70°S and created an additional 2.4 million km^2 of ozone hole area in September 2015 by using the WACCM model. Conversely, Zuev et al. (2018) supports the assumption that the stratospheric volcanic aerosols from the moderate magnitude eruption of Calbuco could not contribute to the intensification of ozone depletion. By combining the ERA-Interim reanalysis data and the Hybrid Single Particle Lagrangian Intergrated Trajectory (HYSPLIT) model, it was found that the volcanic plume was outside the stable polar vortex. Zuev et al. (2018) concluded that the cause of the abnormal stratospheric ozone depletion above Antarctic during October and November was due to the behavior of the polar vortex in that period. Through the analysis of the zonal average backscattering from CALIOP, Zhu et al. (2018) showed that the

Calbuco aerosols progressed toward the South Pole at 16 km during June. Moreover, Bègue et al. (2017) discussed the meridional spread of the Calbuco aerosols toward the South Pole, which was modulated by the Quasi-Biennal Oscillation.

The present paper reports on the sunphotometry observations of the Calbuco plume at 6 South American and 3 African sites. The geographical localization of these sites is helpful to improve the discussion on the latitudinal distribution of the Calbuco plume. Following the Puyehue-Cordon Caulle eruption, an effort was made to deploy CIMEL sunphotometer system over Argentina in order to detect aerosols from volcanic ash and Patagonia dust (Otero et al., 2015). These new databases integrated into the Aerosol RObotic NETwork (AERONET) global network since 2012 and 2013, will be used and analyzed in this study. The usefulness of the sunphotometry measurements on the investigation of the aerosols from major and moderate eruptions has been reported in many previous works (Hobbs et al., 1982; Gooding et al., 1983; Deshler et al., 1992; Watson and Oppenheimer, 2000, 2001; Porter et al., 2002; Mather et al., 2004; Sellitto et al., 2017, 2018). Most of these previous works report on the investigation of optical properties young volcanic plumes near to the source regions. The aims of this study are to quantify the influence of the Calbuco plume on the total columnar aerosols and to discuss on the spatio-temporal evolution of the optical properties of the volcanic plume during its transport. The paper is organized as follows: Section 2 describes the observations and the statistical approach used to investigate the transport and the optical characteristics of the plume. A description of the transport of the Calbuco plume is given in Section 3. The statistical detection of the volcanic plume and its contribution on total columnar aerosols are provided in Section 4. The discussion on the spatio-temporal evolution of the optical properties of the volcanic plume during its transport is presented in Section 5. A summary and the perspectives of this study are given in Section 6.

2. Data and methodology

2.1 Aerosols and Sulphur dioxide observations

The ground-based sites selected to analyze the transport and the optical characteristics of the volcanic plume include 9 AERONET sites in south America and southern Africa: Sao Paulo (23.3°S, 46.4°W), Gobabeb (23.3°S, 15.0°E), Pretoria (25.4°S, 28.1°E), Durban (29.5°S, 31.0°E), Buenos Aires (34.4°S, 58.2°W), Neuquén (38.5°S, 68;0°W), Bariloche (41.0°S, 71.2°W), Comodoro (45.5°S, 67.2°W), and Rio Gallegos (51.3°S, 69.1°W). The localization of these sites in the Southern Hemisphere allows for a large-scale view of the transport of the volcanic aerosol plume. Measurements are obtained at 15-min interval under cloud-free and day time conditions. The direct solar extinction and diffuse sky radiance measurements are used to compute AOD and to the retrieve aerosol size distribution using the methodology of Dubovik and King (2000). The estimated uncertainty in AOD measurements under cloud free condition range from 0.01 to 0.02 (Dubovik et al., 2000, 2006; Eck et al., 2003, 2005). A detailed description of the CIMEL sunphotometer of the AERONET network and the associated data retrieval is given by Holben et al. (1998). The AOD values presented in this work are selected at Level 2.0 (Cloud-screened and quality assured) and downloaded at: http://aeronet.gsfc.nasa.gov/. All available observations performed before the Calbuco eruption until 2016 are also used for this work. The available daily observations and the associated period for each sitesare reported in Table 1. The available daily observations range from 242 to 3237 at Durban and Buenos Aires, respectively (Table 1). The difference between these sites is mainly due to their activity period. It is worthy to note that measurements were made quasi-continuously at each site during the period selected for this study.

During the eruption ***lidar*** measurements were also performed at the Bariloche site, which is located nearest the Calbuco volcano (less than 90 km). The ***lidar*** installed at the Bariloche airport uses a ND:YAG laser emission system based on Quantel Brilliant B 20 Hz laser, with 366 mJ at 1064 nm (Ristori et al., 2018). The collection of the backscattered photons is done with a 20 cm Cassegrain telescope connected via an optical fiber to a spectrometric box. The system can detect the 3 elastics lines: 355, 532 and 1064 nm, two Raman lines 387 and 607 nm, and water vapor at 408 nm. In this study, elastics ***lidar*** signals from 532 nm were processed to retrieve the extinction profile (Fernald, 1984). ***The Klett-Fernald-Sassano (KFS) method was applied as the inversion algorithm. The analytical solution obtained from the KFS method assumes a constant relation between the extinction-to-backscattering profiles, named lidar-ratio (LR) which is a key point of this method. The LR value is obtained from the values reported in the literature in link with the nature of the aerosols (Trickl et al., 2013; Ridley et al., 2014; Sakai et al., 2016) or iteratively by using a reference AOD given by Sunphotometer. In this study, we used the AOD given by the sunphotometer deployed at the Bariloche site. Another parameter that we need to retrieve the optical properties is the altitude reference which correspond to altitude without aerosols load. The statistical uncertainties of the optical products are calculated based on a Monte Carlo method (D'Amico et al, 2015), widely used in EARLINET (European Aerosol Research LIdar NETwork) Network. The systematics errors related to the inversion method are mainly related to the inputs parameters: LR and altitude reference values. On average, errors related to altitude reference is 15%, and those related to LR is around 20%.***

The Moderate Resolution Imaging Spectroradiometer (MODIS) is an instrument aboard the Terra Earth observation system (EOS AM) and Aqua (EOS PM) satellites. The orbit of Terra is timed so that it passes over the equator from north to south in the morning. The orbit of Aqua is timed so that it passes over the equator from north to south in the afternoon. MODIS provides radiance measurements in 36 spectral bands between 0.44 and 15 μm, with different spatial resolution: 250 m (bands 1 and 2), 500 m (bands 3 - 7) and 1 km (bands 8 - 36) (Bennouna et al, 2013). MODIS aerosols retrievals are done separately over land and ocean using two independent algorithms (Bennouna et al, 2013). Numerous works such as Kharol et al. (2011), El-Metwally et al. (2010) and Baddock et al. (2009) have presented a comprehensive description and operation of the Terra MODIS. ***In this study, the MODIS data aboard the Terra (EOS AM) satellite were used and downloaded from:*** https://giovanni.gsfc.nasa.gov/giovanni/. In this study, MODIS AOD data were collected for 2002 - 2016 period over an area of 0.5° x 0.5° latitude and longitude centered on each site to analyze local as well as regional aerosols loadings. We use high resolution MODIS retrievals with only very good quality flags to generate AOD statistics over these regions. Taking into account the conditions mentioned previously the daily observations ranges from 1204 to 3731 at Rio Gallegos and Durban, respectively (Table 1).

The Cloud-Aerosol Lidar with Orthogonal Polarization (CALIOP) onboard the Cloud-Aerosol Lidar and Infrared Pathfinder Satellite Observation (CALIPSO) was used to study the transport of the Calbuco plume. CALIPSO flies in a sun-synchronous polar orbit since 2006 with a cycle of 16 days (Winker et al., 2009). In addition to CALIOP, CALIPSO is composed of two other instruments: (i) The Imaging Infrared Radiometer (IIR); (ii) The Wide Field Camera (WFC). CALIOP is an elastically backscattered ***lidar*** operating at 532 nm and 1064 nm, equipped with a depolarization channel at 532 nm. Moreover, CALIOP can be categorised into two level products; level 1 and level 2. The level 1 products are made up of calibrated and geo-located profiles of the attenuated backscatter returned signal. Level 2 products, on the other hand, are derived from level 1 products and are classified in three types: profile, vertical feature mask and layer products ***(Lopes et al., 2012)***. Layer products provide layer-averaged properties of detected aerosol and cloud. Profile products provide retrieved extinction and backscatter profiles within these layers. The data products are provided at various spatial resolutions. A detailed description of CALIPSO is given in Winker et al. (2009, 2010 and 2013). In this work the analysis of the 532 nm aerosol extinction coefficient data product for the period from 23 April to 3 May 2015 was used for the identification of volcanic plumes in the respective days of observation.

The Ozone Monitoring Instrument (OMI) data product OMSO2G is also used to analyse the transport of the SO_2 plume from the source region to South Africa. OMI is a nadir viewing spectrometer aboard the National Aeronautics and Space Administration (NASA) EOS AURA satellite since July 2004. The AURA satellite occupies a near polar sun-synchronous orbit at an altitude of 705 km (Krotov et al., 2016). A full technical description of the OMI data product is given in the OMI Algorithm Theorical Basis Document (Barthia et al., 2002). OMSO2G products used in this work are selected at Level 2.0 with version 3 and are accessible from: http://disc.sci.gsfc.nasa.gov/Aura/data-holdings/OMI/. The OMSO2G products are obtained from reflected solar radiation measured in spectral ranges 310-340 nm. The data used in this work are reprocessed with the new algorithm based on Principal Component Analysis (PCA) (Li et al., 2013) reducing by half the retrieval noise compared to the previous version. The OMSO2G products are available for four vertical distributions in sampling grid of 0.125° x 0.125° latitude and longitude (Krotov et al., 2016). The Stratospheric Layer (STL) dataset is used for this investigation. Earlier works reports that this dataset is suitable for studying volcanic eruptions (Sangeetha et al., 2018; Li et al., 2013; Krotov et al., 2016). The estimated uncertainty in SO_2 values under cloud free condition for the four vertical distributions is ranging 0.1-0.4 DU and 0.7-0.9 DU at equatorial and high latitudes respectively.

2.2 Back-trajectory model: HYSPLIT

The HYSPLIT model was used to calculate backward and forward trajectories in order to derive information on the transport of the volcanic aerosol plume. The National Oceanic and Atmospheric Administration (NOAA) Air Resource Laboratory (ARL) developed the HYSPLIT model that is being used for computing simple and complex air parcel trajectories (Draxler and Rolph, 2003; Stein et al., 2015). The model can further give information on the dispersion, chemical transformation and deposition simulations of pollutants. The ability of HYSPLIT to derive information on the atmospheric transport, dispersion and deposition of pollutants and volcanic ash has been highlighted in several studies (Stunder et al., 2007; Chen et al., 2012; Kumar et al., 2017; Sangeetha et al., 2018; Lopes et al., 2019; Shikwambana and Sivakumar, 2019). A detailed description and its historical evolution is given by Stein et al. (2015) and is briefly presented here. The calculation of the trajectories is based on hybrid method between the Lagrangian and Eulerian approaches (Stein et al., 2015). In order to reduce the uncertainties induced by the meteorological fields and the numerical methods employed, HYSPLIT can be run in the trajectory clustering mode. The concept of clustering is a multivariate statistical method which consist in merging the trajectories that are closer to each other and class them into distinct group. In the present work, the back-trajectories calculations were helpful to determine if the measured AOD over the selected sites are associated to air masses that come from the Calbuco volcano. The back-trajectories of air-masses were calculated every 6h over the selected sites using the Global Data Assimilation System (GDAS) database for altitudes ranging from 16 to 19 km. The back-trajectories calculations were performed using the vertical motion calculation method.

2.3 Methodology

The characteristics of the optical properties of the volcanic plume were analyzed using AOD measurements. The AOD measurements are comprised of the volcanic plume AOD_P and the background values. Thus, the aerosols optical depth of the volcanic plume at a given wavelength AOD_P (λ) can be obtained by subtracting the background aerosols optical depth AOD_B (λ) to the AOD (λ) measurements. This methodology has been applied on the Microtops II portable sunphotometer measurements taken close to volcano site (Watson and Oppenheimer, 2001; Porter et al., 2002; Mather et al., 2004; Martin et al., 2009; Sellitto et al., 2017, 2018). In this paper, this approach was applied and adapted to CIMEL sunphotometer measurements taken at 9 sites. To investigate the properties of the volcanic plume, it is important to make background measurements when the atmosphere is clear of volcanic aerosols as well as measurements during an eruption. Given that CIMEL sunphotometers are fixed instruments, this requirement is implicitly respected and allows to define a background situation statistically significant. In the present work, the background period is defined as the period before January 2015 and after January 2016. Except for the Durban site, AOD_B (λ) calculation is based on an average of 6 years of daily observations (Table 1). The anomalies were filtered out in order to obtain daily optical depth of the “clear” atmospheric layer. Thus, the calculated daily of AOD_B (λ) means from April to December were assumed to be within the standard deviation of hourly recorded data. Moreover, the perturbation induced by the Puyehue Cordon Caulle eruption (40.3°S; 72.1°W, Chile) (Diaz et al., 2014) on the calculation of the background values was taken into account. As a consequence, the measurements performed during the period ranges from June to October 2011 were discarded to the calculation of the AOD_B (λ). Taking into account the conditions mentioned previously the number of observations used for the calculation of the daily AOD_B (λ) means ranges from 89 to 2489 (Table 1). The uncertainty of the in-plume AOD (σ_{AODp}) is derived by using the standard deviation of the AOD (λ) measurement and the standard deviation of the AOD_B (σ_{AOD_B}), as shown by Sellitto et al. (2017). This uncertainty is given by equation (1):

$$\sigma_{AOD_P}(\lambda) = \sqrt{\sigma_{AOD}{}^2 + \frac{\left(\sigma_{AOD_B}\right)^2}{n}} \qquad (1)$$

With n the number of individual background measurements AOD_B made to compute the average background.

The spectral variability of the volcanic plume was analyzed by using the Angström exponent α_P and the atmospheric turbidity β_P (Angström, 1964). The Angström exponent α_P is a well-known optical proxy for the aerosol size distribution (Shaw, 1983; Tomasi et al., 1997). The Angström exponent α_P is generally close to zero or negative for aerosols whose extinction properties are governed by large particles (mean radius distribution greater than 1 µm). Conversely, α_P values greater than 1 are typical of small particles (mean radius distribution less than 1 µm). The Angström turbidity β_P is the best fit value of AOD_P (λ) at 1 µm which depends on the total number and refractive index of aerosols particles. In this present work, the optical properties of the volcanic plume were analyzed at three selected wavelength bands which correspond to ultraviolet (380 nm), visible (500 nm) and near-infrared (1020 nm). Previous works revealed that the observations in UV wavelengths are helpful for the characterization of the optical and microphysical properties of the volcanic plume (Porter et al., 2002; Mather et al., 2004; Sellitto et al., 2017). The Angström exponent α_P and turbidity β_P of the volcanic plume are calculated at selected wavelength pair 380-1020 nm, given by equations (2) and (3):

$$\alpha_P = -\frac{ln\left[\frac{AOD_P(\lambda_1)}{AOD_P(\lambda_2)}\right]}{ln\left[\frac{\lambda_1}{\lambda_2}\right]} \qquad (2)$$

$$\beta_P = AOD_P(\lambda_1).\,\lambda_1{}^{\alpha_p} \qquad (3)$$

As reported by Sellitto et al. (2017), the use of a spectral interval as large as possible, led to a decrease in the uncertainties content of α_P and β_P. According to this research, the uncertainties of the derived α_P and β_P are calculated as follow:

$$\sigma_{\alpha_p} = \left[\frac{1}{ln\left(\frac{\lambda_1}{\lambda_2}\right)}\right] \sqrt{\left(\frac{\sigma_{AOD_P}(\lambda_1)}{AOD_p(\lambda_1)}\right)^2 + \left(\frac{\sigma_{AOD_P}(\lambda_2)}{AOD_p(\lambda_2)}\right)^2} \qquad (4)$$

$$\sigma_{\beta_p} = \lambda_1{}^{\alpha_p} \sqrt{\left(\sigma_{AOD_P}(\lambda_1)\right)^2 + \left(AOD_p(\lambda_1).\ln\lambda_1\right)^2 \sigma_{\alpha_p}{}^2} \quad (5)$$

The spatio-temporal data analysis carried out between MODIS and sunphotometer instruments helps both to detect the passage of the volcanic plume and its contribution to the total aerosol column variation, over the selected sites. The methodology described previously, was applied to the MODIS observations in order to determine the AOD of the volcanic plume $AOD_{P\text{-}modis}$ and the background values $AOD_{B\text{-}modis}$ at 550 nm. MODIS observations are helpful to obtain a good description of the background behavior over the sites where sampling is not sufficient, such as the Durban. Table 1, reveals that the MODIS observations used to build the background situation ***are homogenous*** between the different sites and range between 689 and 3216. It is necessary to convert the AOD values from MODIS and sunphotometer to a common wavelength in order to compare them. The AOD values obtained from sunphotometer at 500 nm were converted to the MODIS wavelength following Equation (6) which has already been used in previous works (Prasad and Singh, 2007; Alam et al., 2011)

$$AOD_{Modis} = AOD_{Photometer} \left(\frac{\lambda_{Modis}}{\lambda_{Photometer}}\right)^{-\alpha} \qquad (6)$$

Where α is the Angström parameter obtained from sunphotometer at 440-870 nm.

3. Long-range transport of the volcanic plume

Figure 1a, depicts a time averaged map of OMI STL SO_2 column between 22 April and 1 May. It is clearly shown that SO_2 injected into the atmosphere is mainly transported northeastward over South America and pass over the Sao Paulo site. This figure also reveals a lack of SO_2 observations over a region spanning from the vicinity of the Calbuco site to southern parts of Argentina. This blind region obtained from OMI observations has already been reported in previous studies as a result of reduced signal-to-noise ratio due to exposure of the low-orbiting satellite instrumentation to radiation and high energy particles (Fioletov et al., 2016; Shikwambana and Sivakumar, 2019). Bègue et al. (2017) pointed out a lack of SO_2 observations over this same region by the use of IASI measurements. ***Over South America, the highest values of SO_2 (2-2.5 DU) are found over Southern Brazil and northern parts of Argentina.*** It can be observed that the outflow of the SO_2 plume towards the Atlantic Ocean is located over the region aforementioned. The plume is transported by the general circulation over the Atlantic Ocean and reached the African region. Large values of SO_2 (2-3 DU) are mainly observed during the transport of the plume over the South Atlantic. The SO_2 plume entered the western parts of South Africa and spread eastward. Figure 1a, reveals that SO_2 plume was transported over South Africa. ***The observed SO_2 values over South Africa are around 3 times weaker***

than those observed over South America and Atlantic Ocean. The SO2 plume progressively moved away resulting in a decrease in amplitude as expected by the oxidation of SO_2 to gaseous sulphuric acid which further condensed into H_2SO_4-H2O liquid aerosol (Bègue et al., 2017).

Forward trajectories starting at the Calbuco volcano on 22 April at 14:00 UTC were calculated for a period of 10-days at three different altitudes between 16 and 20 km (Fig. 1b). It is worthy to note that the trajectories calculated by HYSPLIT model are in fair agreement with the shape of the SO_2 plume obtained with OMI observations for the same period. Figure 1b reveals that the air masses from the Calbuco site leave the South American region on 26 April for the three selected altitudes. ***It can be observed that the outflow of the air masses from Calbuco towards the Atlantic Ocean is located over Southern Brazil and northern parts of Argentina for the three selected altitudes (Fig. 1b). It is worthy to note that this spread of the air masses from Calbuco obtained from HYSPLIT model is consistent with the spread of the SO_2 plume obtained from OMI observations.*** Over the Atlantic Ocean, the spatio-temporal distribution of the air masses from the Calbuco site depends on the given altitude. The original air masses from the Calbuco site at 16 km reached the southwestern parts of South Africa from 30 April at around 16.5 km. These air masses travelled to eastern parts of South Africa one day later and reached the south-western Indian Ocean on 1 May at 16.9 km. Conversely, the original air masses from the Calbuco site at 18 and 20 km reached the western and the southern parts of South Africa, on 1 May. ***The trajectories analysis reveals that the air masses from Calbuco are advected eastward and mainly in the Southern Hemisphere. This result is found in agreement with published previous results (Bègue et al., 2017; Shikwambana and Sivakumar, 2018; Zhu et al., 2018). Bègue et al. (2017) showed that the latitudinal extent of the Calbuco plume was bounded by the subtropical barrier and the polar vortex. The air masses from Calbuco was advected between South America and South Africa following the wave shape of the dynamical barriers (Bègue et al., 2017).***

Figure 1c, further shows a time averaged map of MODIS AOD at 550 nm between 22 April and 1 May. ***The AOD values in coincidence with the forward trajectories calculated from HYSPLIT model could be explained by the presence of the Calbuco plume. Thus, the synergy between the forward trajectories and MODIS observations allows to determine the AOD values in link to the Calbuco eruption. It can be deduced that large values of AOD (0.6 - 1) mainly observed over the South American region in the vicinity of the Neuquén site are linked to the Calbuco eruption (Fig. 1c). Analysis of the forward trajectories and the MODIS observations, also indicate that a large values of AOD (0.6 - 0.8) around to the African region***

are in coincidence with the Calbuco plume pathways. Over the Atlantic Ocean, the AOD values associated to the passage of the Calbuco plume range between 0.4 and 0.8.

The daily extinction coefficients at 532 nm observed by CALIOP between 17:30 UTC to 18:40 UTC on 23 April over the Calbuco volcano and Sao Paulo site are depicted in Figure 2. High extinction coefficients values (greater or equal to 0.35 km^{-1}) are observed in the vicinity of the Calbuco volcano and the Neuquén site between 14 and 18 km (Fig. 2a). The back-trajectory analysis clearly indicates that this thick aerosol layer observed by CALIOP is connected to the Calbuco eruption. The aerosol plume is structured in two layers separated by weak extinction coefficients values (0.01-0.02 km^{-1}). The first layer is found between the Calbuco volcano and the Bariloche site with a vertical extent from 14 to 18 km. The second layer is centered over the Neuquén site with weaker vertical extent ranging from 15.5 to 18 km. This two-layer structure of the plume indicates its inhomogeneity at this stage. One day later, the volcanic aerosols layer is observed between the Neuquén and Buenos Aires sites and structured into one compact layer extent spanning from 16 to 18 km (Fig. 2b***). On 26 April, extinction coefficients values greater or equal than 0.15 km^{-1} in link with the Calbuco eruption are observed near to the Sao Paulo site between 18 and 20 km (Fig. 2c). The altitude of the high extinction coefficients values is in agreement with the results obtained by Lopes et al. (2019) from lidar observations over the Sao Paulo site.*** The spread of the plume over the northeastern parts of South America is associated with a decrease in thickness. This decrease could be explained by the sedimentary process which impacted mainly the coarse aerosol particles such as volcanic ash near to source region. Figure 2, reveals that the top layer aerosols increase slightly during its transport toward the northeast parts of South America from 23 to 26 April. The feature of the volcanic aerosol plume over the African region is investigated from the daily extinction coefficients at 532 nm observed by CALIOP over a region extended from (23° S, 15° E) to (29°S, 31°E) (Fig. 3). On 30 April, a thin discontinuous aerosols layer (less than 1 km) extended from west to east is visible on CALIOP observations (Figure 3a). Highest extinction values (0.05-0.07 km^{-1}) are found mainly on the western parts of southern Africa in the vicinity of the Gobabeb site, whereas weakest values (0.02-0.03 km^{-1}) are observed on the eastern parts in the vicinity of the Durban site. This suggests that the volcanic plume reached the western parts of Southern Africa few days later (as shown above) and it followed its propagation by reaching the eastern side on 30 April. Three days later, an increase of the extinction values and the thickness of volcanic plume is hence observed in the vicinity of the Durban (Fig. 3b). Conversely, dilution of the volcanic plume is associated with a decrease by half of the extinction values over the western parts of South Africa. The observed extinction values over South America are around 10 times higher than those observed over South Africa (Fig. 2 and Fig. 3).

Overall, the satellite observations indicate that the majority of the aerosol plume is injected in the lower stratosphere and propagated toward South Africa during the week following the eruption. It also seems that the southern parts of Argentina were not influenced by the volcanic plume during this period of time. The synergy between the satellite and ground-based observations reinforce the description of the latitudinal distribution of the volcanic plume. The detection of the volcanic plume from the ground-based observations is discussed in detail in the next section.

4. Influence of the Calbuco plume on the total columnar aerosols

4.1 Statistical detection of the volcanic plume

Figure 4 and Figure 5, depict the daily mean evolution of AOD at 550 nm obtained from sunphotometer and MODIS observations at 6 South American sites between 15 April and 1 December. The selected sites allow for an overview of the latitudinal distribution of AOD over the South America region. These sites are located in urban and semi-urban areas dominated by industrial activities and local air pollution (e.g., vehicle emission, air traffic). It appears a north-south gradient in the background values of AOD obtained from sunphotometer and satellite observations over South America region (Fig. 4 and Fig. 5). The background values of AOD and its variability decrease with higher latitudes. The annual mean of AOD background from Sao Paulo to Rio Gallegos are ranging between 0.11 ± 4.10^{-3} and 0.03 ± 1.10^{-3} respectively. The highest values of AOD (with annual mean greater or equal than 0.10) and largest variability are observed at Sao Paulo and Buenos Aires (Figures 4a-b and Figures 4c-d) respectively. These regions are the most industrialized of the selected Southern American sites (Gassman et al., 2000; Lopes et al., 2019). The AOD values over the Neuquén site which is located 4 degrees south to Buenos Aires, is on average half of that those observed, at Buenos Aires (Fig. 5a and Fig. 5b). In addition to urban and industrial activities, the evolution of the background values over Sao Paulo and Buenos Aires is influenced by the biomass burning activity which explain the increase in AOD values during the Austral winter (June-August) (Andreae et al., 2004; Freitas et al., 2009; Torres et al., 2010). Based on sunphotometer observations over the South America, Hoelzemann et al. (2009) showed a clear difference on the AOD behavior between purely fires and urban influenced sites. This explains the contrast between the Northern and Southern parts of South America. The South American region is influenced by the regional and long-range transport of air masses from several potential sources of aerosols which induce seasonal variability on optical properties of aerosols over the country. For instance, the transport of dust from Patagonia region impacts the seasonal variability on optical properties of aerosols of the neighbor sites such as Comodoro (Li et al., 2010; Otero et al., 2015). Moreover, the southern parts of Argentina are frequently impacted by air masses from Antarctic, which could influence the variability of AOD over Rio Gallegos (Kirchhoff et al., 1997; Otero et al., 2015). We cannot exclude the hypothesis that the increase of AOD values observed from sunphotometer and MODIS measurements performed at Rio Gallegos during the Austral winter could be explained by the transport of air masses from Antarctic region (Figure 5e and Figure 5f). Figure 6a reveals that the background values of AOD and its variability over Sao Paulo and Buenos Aires compare fairly well with the observed values over the Gobabeb site (in average $0.10 \pm 6\ 10^{-3}$). The background values of AOD observed at Gobabeb are slightly lower than those observed at Durban (in average 0.16 ± 8.10^{-3}) and Pretoria (in average 0.17 ± 8.10^{-3}) both by sunphotometer and MODIS (Figure 6). The Gobabeb site, in the Namib Desert, is far less sensitive to the effect of urban pollution than the Durban and Pretoria sites. It can be observed that all these African sites exhibit an increase of the AOD values during the Austral spring season which is well-known to be the biomass burning season (Eck et al., 2003; Garstang et al., 1996; Das et al., 2015; Piketh et al., 1999; Kumar et al., 2017).

The daily AOD measurements performed between 15 April and 1 December 2015 were compared to background values in order to highlight the passage of volcanic plume. Furthermore, back-trajectory analysis of daily AOD measurements of 2015 found higher than background values were made in order to link observations with the Calbuco plume. It is therefore possible to determine the duration of the plume over a specific site. This duration is defined as the period during which AOD measurements from 2015 fall outside the standard deviation of the daily background means. The duration of stay of the Calbuco plume detected from total columnar aerosols measurements is reported on Table 2 and depicted by the grey shaded area on Figures 4, 5 and 6. The estimation for the duration of the plume depends mainly on the availability of daily observations. This condition results in the discrepancies between the duration of stay between the MODIS and sunphotometer observations. Given its good temporal resolution, the daily comparison between the observed AOD by MODIS during the background period and Calbuco event are possible during a long period of time. Measurements collected by these two instruments are complementary and allow to improve the estimation of the duration stay over the selected sites. This is clearly illustrated with the case of the Bariloche site where no measurements were recorded by the sunphotometer from 26 April to 10 May during the background period ***(Fig. 4e and Fig. 4f).*** The use of MODIS observations has allowed to improve the estimation of the duration stay and conclude that the duration of stay of the plume was from 23 April to 10 May 2015. In spite of the large variability of the background values over the Sao Paulo and Buenos Aires sites, the passage of the volcanic plume is clearly visible from the sunphotometer and MODIS observations (Fig. 4a-b and Fig. 4c-d). This previous comment is also true for the African sites (Fig. 6). It is worthy to note that the duration of stay obtained for these sites are in agreement with the chronology reported in the previous subsection from CALIOP and OMI observations. It can be observed that the passage of the volcanic plume is not clearly visible over the southern parts of the South American region. Figure 4e reveals that the passage of the Calbuco plume over the Rio Gallegos site is not visible from AOD measurements recorded by the sunphotometer. This could be explained by the low daily sampling during 2015. Conversely, the AOD measurements recorded by MODIS from 12 to 25 May 2015 are higher than daily background values (Fig. 5f). The air masses back-trajectory calculations confirm the link of these observations with the Calbuco eruption, in agreement with those reported by Zuev et al. (2018). They analyzed the trajectory of air masses calculated with the Calbuco volcano from 22 April until the end of August between 15 and 19 km using the NOAA HYSPLIT model. Zuev et al. (2018) showed that air masses were within limits of the subtropical stream and polar vortex, impacting the southern parts of the South America. However, the MODIS observations aforementioned are within the standard deviation of daily background mean. As a consequence, it is impossible to determine a duration stay over the Rio Gallegos site following the statistical criteria defined previously. ***Figures 5e and 5f***, do not call into question the passage of the volcanic plume over the Rio Gallegos site but rather suggest that the AOD measurements are not statistically significant. A possible explanation for this is that amount of aerosols transported toward Rio Gallegos are lower than the amounts transported toward the northern parts of South America which reach South Africa a few days later. The lower amount of volcanic aerosols gets lost in the variability of the background values. In the following subsection, the contribution of the volcanic plume on the total columnar aerosols will be discussed in more details.

4.2 Statistical variations of the total columnar aerosols

The daily AOD anomalies induced by the transport of the volcanic plume are estimated and calculated as a relative difference by considering the daily background as the reference values. The Bariloche site is clearly the most exposed to the volcanic plume which is illustrated by the significant difference (in average a factor of 2.5) between the daily AOD measurements of 2015 and background values (Figure 4e). During the first days following the eruption, the AOD values obtained by ***lidar*** and sunphotometer observations ranges from 0.18 to 0.24 (Fig. 4e). This validates that these high values are not as a result of technical artefacts, but attributed to the passage of the Calbuco plume detected by two ground-based independent instruments. The maximum values of the relative difference are observed over the Bariloche site (Fig. 7c and Fig. 7d). Figures 7c and 7d, reveal that the AOD anomalies calculated from the sunphotomoter and MODIS observations during the first days after the eruption range from 35 to 85 %. Despite of its geographical distance to the Calbuco volcano site and its significant background variability, the passage of the plume over the Sao Paulo site has induced a significant daily AOD anomalies ranging from 20 to 55 % (Fig. 7a and Fig. 7b). The African sites situated in the west, such as Gobabeb were first impacted by the volcanic plume and AOD anomalies induced by its spread are significant. Over the Gobabeb site, the daily AOD anomalies range from 10 to 55 % (Fig. 7e and 7f). Table 2, contains the mean values of the AOD anomalies calculated during the duration stay over all the selected sites. Overall, the AOD anomalies induced by the passage of the plume over the South American sites are on average higher than those obtained over Southern Africa sites (Table 2). This is consistent with the contrast on the extinction coefficient obtained by CALIOP between South America and South Africa reported in the previous subsection. Table 2, reveals that the highest AOD anomalies (greater than 35 %) are observed over the northeastern parts of South America, enclosing the Bariloche, Neuquén, Buenos Aires and Sao Paulo sites. The AOD anomalies for the Comodoro site, which is south to the Calbuco site, are estimated to at 26.4 ± 1.5 % and 14.5 ± 2.5 % from sunphotometer and MODIS, respectively. There seems to be a difference between the sites located to the north and south of the Calbuco volcano with regards to the AOD anomalies induced by the passage of the plume. It is worthy to note that latitudinal distribution of AOD anomalies over South America is consistent with the geographical spread of the volcanic plume obtained by satellite observations. Both the satellite and ground-based observations reveal that the majority of the volcanic plume was transported over the northeastern part of South America during the first days following the eruption. Conversely, the AOD anomalies induced by the spread of the plume from west to east over South Africa have a homogeneous distribution. On average, the AOD anomalies for Gobabeb and Durban are estimated at 22.5 ± 13.0 % and 24.8 ± 11.1 %, respectively from sunphotometer observations, and estimated at 20.1 ± 11.2 % and 27.5 ± 10.8 %, respectively from MODIS observations (Table 2). On average, the difference between AOD anomalies obtained from MODIS and sunphotometer observations is less than 7% with the exception of the Comodoro site for which the difference is estimated to be 11.9 %. The discrepancies in term of AOD anomalies between MODIS and sunphotometer may be attributed primarily to the estimation of the duration stay as previously mentioned. It is important to note that the discrepancies from background measurements from MODIS and sunphotometer should not be excluded.

The correlation coefficient and mean bias error (MBE) between sunphotometer and MODIS AOD observations are depicted in Figure 8 and reported in Table 3. The correlation coefficient values range from 0.51 to 0.76 with the highest correlation observed over the Pretoria site (Fig. 8c and 8d). This is in agreement with previous studies which reveal that the correlation is significant between MODIS and sunphotometer over the land instead of over the ocean and coastal sites due to its low surface reflectivity characteristic (Chu et al., 2002; Vermote et al., 1997; Hoelzemann et al., 2009; Bréon et al., 2011). It is worthy to note that the correlation between the sunphotometer and MODIS observations over the Sao Paulo site is similar to those observed over Durban and Pretoria (Fig. 8a and 8b). In addition, the root mean square error (RMSE) was calculated and is reported in Table 3. The RMSE and MBE values range from 4.2 % to 13.2 % and from - 9.7 % ± 3.2 % to 8.2 % ± 0.9 %, respectively. The highest discrepancies between the sunphotometer and MODIS measurements (correlation coefficient lower than 0.60 and RMSE greater than 9%) are observed in the southern parts of South America, close to the Comodoro and Rio Gallegos sites. In particular, the Comodoro site has the weakest correlation (0.51) and MBE values of - 9.7 % ± 3.2 % (Fig. 8e and 8f). Previous studies have already pointed out the bias in AOD data sets collected by MODIS and ground-based instruments in the Southern Hemisphere between 45°S and 65°S (Zhang and Reid, 2006; Shi et al., 2011; Lehahn et al., 2010; Madry et al., 2011; Toth et al., 2013). Madry et al (2011) suggested that this bias could be due to the production of sea-salt particles by the near-surface high winds occurring along this zonal band. Toth et al. (2013) investigated the quality of MODIS data sets in this zonal band by comparing them with CALIOP and sunphotometer observations. They showed about 30-40 % of the observed bias with the ground-based observations could be attributed to cloud contamination. Table 3, reveals that MODIS overestimates the AOD when compared to sunphotometer for most part of the selected sites which is consistent with previous studies (Ichoku et al., 2005; Abdou et al., 2005; Hauser et al., 2005; Hoelzemann et al., 2009). This bias may be explained by the fact that sunphotometer measurements are made under cloud-free conditions, whereas MODIS is able to detect aerosols under cloudy pattern. However, subpixel cloud can be targeted as aerosols which erroneously raise the retrieved AOD (Hoelzemann et al., 2009). Conversely, we note that MODIS underestimates the AOD when compare to sunphotometer over the Sao Paulo and the South African sites (Table 3). For the latter, this was found to be consistent with results obtained by Hao et al. (2005) during the

Southern African Regional Intensive (SAFARI 2000) campaign showing that in the regions of intense biomass burning, AOD values from MODIS are systematically lower at 470 nm, 550 nm, and 660 nm compared to ground-based measurements by automated and handheld sun photometers. They suggested that this bias may be due to errors in the assumed aerosol scattering phase function or surface directional properties. Thus, several potential causes (surface reflectance, cloud contamination, retrieval bias) could contribute to the discrepancies between MODIS and sunphotometer observations (Tripathi et al., 2005; More et al., 2013; Kumar et al., 2015). The statistical results previously mentioned, indicate that the daily AOD values obtained from sunphotometer and MODIS observations are in fairly good agreement. Overall, the anomalies induced by the transport of the Calbuco plume can be statistically detected and evaluated using the AOD measurements at mid-visible wavelengths. In order to improve the discussion, the observed AOD from the UV to near infrared spectral ranges will be analyzed in the following section.

5. Discussion on the optical characteristics of the volcanic plume

The time evolution of the extinction profile obtained from the collocated LiDAR measurements at 532 nm confirms the presence of the volcanic plume between 12 and 15 km between 24 and 25 April over the Bariloche site (Fig. 9a). The spectral variability of plume isolated AOD (AOD_P) values obtained from sunphotometer observations during the aforementioned period is shown in Figures 9b and 9c. For both days, the AOD_P evolutions are not characterized by a wavelength dependence (Fig. 9b) but are similar to those from the UV and NIR spectral range (average 0.18 ± 0.05). This optical behavior is typical to an aerosol layer dominated by larger particles such as mineral dust or ash particles (Mather et al., 2004; Bègue et al., 2012; Sellitto et al., 2018). The Angström exponent α_P and the uncertainty calculated for the wavelength pair 380 - 1020 nm by using Equations (2) and (4) respectively, are also shown in Figure 9b. The mean values of the Angström exponent α_P on 24 and 25 April are -0.05 ± 0.02 and 0.1 ± 0.06, respectively. ***These values confirm a dominance of larger particles with radius greater than 1 µm (Watson and Oppenheimer, 2000). Time evolution of the Angström turbidity β_P and its uncertainty derived by using Equations (3) and (5) are depicted in Figure 9c. The β_P parameter increases with the number of particles. The Angström turbidity β_P evolution is therefore correlated with the AOD_P values as depicted in Figure 9b. As a consequence, weak β_P-values is consistent with the plume being less thick and weak AODp values. Conversely, high β_P (greater than 0.1: thick aerosol layer) and weak α_P (less than 0.5: coarse particle) can be associated to relevant burdens of larger particles, like for ash puff (Sellitto et al.,***

2018). On average, the Angström turbidity β_P values range from 0.16 ± 0.06 to 0.19 ± 0.04 over the Bariloche site on 24 and 25 April, respectively. For both days, a negative correlation is observed between the Angström exponent α_P and the turbidity β_P. This suggests a significant increase in larger particles over the Bariloche site. ***This negative correlation reveals therefore the presence of a thick aerosol layer dominated by larger particles over the Bariloche site two days after the eruption.*** These results are found to be in agreement with estimations of Angström coefficients for ash-bearing plume reported in previous studies (e.g., Watson and Oppenheimer, 2000, 2001; Porter et al., 2002; Mather et al., 2004; Martin et al., 2009; Sellitto et al., 2017, 2018). During the minor eruption of the Lascar volcano (23.4°S, 67.7°W, Chile) in 2003, the Angström exponent α_P (440-1020 nm) and turbidity β_P derived from Microtops sunphotometer observations for ash-bearing were found to be smaller than 0.3 and ranging from 0.04 to 0.10 respectively (Mather et al., 2004). Through the use of sunphotometer observations during the last Mount Etna (37.5°N, 14.6°E) eruption, Sellitto et al. (2017) found the Angström exponent α_P (380-1020 nm) and turbidity β_P for ash-bearing equal to -0.30±0.22 and 0.08±0.05 respectively. During the eruption of Mount Etna volcano in October 1997, the Angström exponent α_P (440-1020 nm) and turbidity β_P derived from CIMEL sunphotometer observations for ash-bearing range from -0.20 to 0.20 and from 0.16 to 0.65 respectively. It is worthy to note that our Angström coefficients estimations are in agreement to the ash-bearing plume observed at Mount Etna by Watson and Oppenheimer (2001).

Figure 10 illustrates that the optical characteristics of the volcanic plume evolved during its transport. On 29 April, the AOD_p values at the Neuquén site are characterized by a wavelength dependence (Fig. 10a). Figure 10a, indicates that higher AOD_p values are observed in the UV range (ranging from 0.08 to 0.27) than in the NIR range (ranging from 0.08 to 0.03). This optical behavior is typical of an aerosol layer dominated by smaller particles (radius lower than 1 µm). This is confirmed by the Angström exponent α_P values which range from 1.2 to 1.5 (Figure 10a). Figure 10c, reveals that the Angström turbidity β_P values range from 0.02 to 0.062 with a mean value of 0.04 ± 0.02 which suggest the presence of a thin aerosol layer. This Angström coefficients estimation is consistent with ash-free plumes previously observed for other volcanic eruptions (Watson and Oppenheimer, 2000, 2001; Porter et al., 2002; Mather et al., 2004; Martin et al., 2009; Sellitto et al., 2017, 2018). For instance, the Angström exponent α_P (440-1020 nm) and turbidity β_P estimated from Microtops observations during the Pacaya volcano (14.2°N, 90.4°W, Guatemala) eruption in 2011 are in average 1.4 ± 0.7 and 0.05 ± 0.07, respectively. Figure 10b, depicts the AOD_P evolution during the day where the plume reached the Gobabeb site. Over this site, time evolution of AOD_P is both characterized by an increase in the volcanic aerosol burden at all wavelengths and a wavelength dependent on 1 May. Thus, higher AOD_p values are observed in the UV range (ranging from 0.04 to 0.15) than in the NIR range (ranging from 0.03 to 0.05). The Angström exponent α_P range between 0.3 and 1.5 with a mean value of 1.1 ± 0.75. This suggests that the particle size distributions of the plume are not homogenous (Fig. 10b). ***The plume was progressively moved away resulting in a weaker signal which lead to a decrease of β_P and more scattered α_P. The increase of the Angström exponent α_P is correlated with the Angström turbidity β_P (ranging from 0.025 to 0.050) (Fig. 10d). This correlation suggest the presence of a thin aerosol layer dominated by smaller particles over the Gobabeb site.*** These Angström coefficients values are also in consistent with the ash-free plume spread over the Gobabeb site, on 1 May (Fig. 10d).

Overall, the ash-bearing plume is characterized by a thick plume containing large particles (α_P < 0.30 and β_P > 0.16) are mainly located near the Calbuco site (such as Bariloche) during the first days of the eruption (24-25 April). Due to the sedimentation process, these large ash particles fall out quickly nearby the source region. The fraction that survives to the near-source fall-out processes are transported over long-range distance. The remote sites to the Calbuco volcano are hence influenced by this ash-free plume characterized by thin plume composed of small particle ($\alpha_P \geq 0.3$ and $\beta_P < 0.15$). These results are consistent with previous studies indicating that the volcanic plume is dominated by larger particles near the source (Hobbs et al., 1982; Rose et al., 2000; Watson and Oppenheimer, 2000; Webster et al., 2012). Rose et al. (1982) showed that this phenomenon could be explained by competing mechanisms involving the adsorption of smaller particles by ash. As reported by Sparks et al. (1997), the aggregation processes are more important near the source. The evolution of the plume thickness obtained from sunphotometer observations are consistent with the evolution obtained from CALIOP observations and presented above in the first subsection. Furthermore, the time evolution of the optical characteristics of the plume over the selected sites was also analyzed through the estimation of the Angström coefficients. Their mean values are reported on Tables 4 and 5. Over the selected sites, the Angström turbidity β_P does not evolve significantly in time and on average is less than 0.06. The Angström exponent α_P tends to decrease slightly in time with exception of the Sao Paulo site for which the Angström exponent α_P stays fairly constant (ranging from 1.1 to 1.3). These values are in agreement with the Ansgtröm exponent α_P retrieved from LiDAR observations over Sao Paulo (Lopes et al., 2019). The slight decrease is clearly visible at the Buenos Aires, Gobabeb and Durban sites for which the Angström exponent α_P is roughly half and reaches on average a value lower than 0.6 (Tables 4 and 5). These low Angström coefficient values suggest that the plume evolves with time so that large-particles dominate the distribution with smaller optical depth. The decrease of the Angström exponent α_P could be due to enhanced particles growth in the plume induced by microphysical processes such as aggregation or coagulation. The balance between the growth and removal process impacts the residence time of the volcanic plume and its size distributions. Moreover, the time evolution of optical properties of the volcanic plume over the selected sites could be also explained by the dynamical context. Indeed, the ageing of aerosols plume is a complex mechanism controlled by many parameters (Bègue et al., 2012; Guermazi et al., 2019).

6. Summary and conclusion

The influence of the Calbuco eruption on the total columnar aerosol optical properties over the Southern Hemisphere has been presented in this investigation. The study focuses mainly on the analysis of the sunphotometer measurements performed at 6 South American and 3 African sites. The satellite observations (MODIS, OMI, and CALIOP) were combined with ground-based observations (sunphotometer and ***lidar***). Moreover, the back-trajectory model (HYSPLIT) was used in order to investigate the transport of the volcanic plume. The spatio-temporal evolution of the volcanic plume obtained from satellite observations was found to be consistent with ground-based time series and in agreement with previous works. It is found that the majority of the plume aerosols were injected up to the lower stratosphere and propagated towards South Africa during the week following the eruption. The spread of the plume over the northeastern parts of South America is associated with a decrease in thickness. The satellite observations pointed out that the southern parts of Argentina are not influenced by the volcanic plume during the first weeks following the eruption. The synergy between the space-based and ground-based observations has allowed for further description of the plume over the southern parts of South America.

The statistical analysis applied on the sunphotometer and MODIS observations pointed out the presence of a north-south decreasing gradient in the background values of AOD over the South America region. The highest values of AOD were observed at the Sao Paulo and Buenos Aires sites which are the most industrialized regions of the selected Southern American sites. The statistical detection of the plume agreed with the chronology of the plume transport obtained from satellite observations. Moreover, this statistical approach revealed that the plume has also impacted the southern parts of South America, albeit in a lesser extent. The anomalies induced by the transport of the Calbuco plume on the total columnar aerosol optical properties was statistically evaluated in mid-visible wavelength. The highest AOD anomalies are observed over the northeastern parts of the South America. Given its proximity to the Calbuco volcano, the Bariloche site was most impacted by the volcanic plume with daily AOD anomalies ranging from 35 to 85 %. Over the South African sites, the AOD anomalies induced by the dispersion of the plume were homogeneously distributed. The observed contrast between the South America and Africa regions was highlighted by the extinction values from CALIOP observations.

From the spectral variability of the plume, only AOD was analyzed from the UV to near infrared spectral ranges. The optical characteristics of the plume near-source region are consistent with a bearing-ash plume. This spectral analysis of the plume reveals an evolution of its optical properties over the remote sites to the Calbuco volcano. Thus, the Angström coefficients values are consistent with an ash-free plume over these sites. The optical evolution of the volcanic plume during its transport is in agreement with previous works (Hobbs et al., 1982; Rose et al., 2000; Watson and Oppenheimer, 2000; Webster et al., 2012; Sellitto et al., 2018) and can be explained by microphysical processes, but also through dynamics (Baker et al., 2014; Bègue et al., 2017.; Guermazi et al., 2019; Nimgomba et al., 2019). The Angström coefficients were useful to obtain a first estimation of the optical characteristics and the size distribution of an aerosol plume. Nevertheless, the Angström coefficients were not sufficient to describe in detail the ageing of the aerosols plume during its transport. The parameters that contributed to the ageing of the Calbuco plume require further investigations which will form the basis for a forthcoming study.

Acknowledgements

This work receives funding by the French Centre National de la Recherche Scientifique (CNRS) and the South African National Research Foundation (NRF) through the "Laboratoire International Associé Atmospheric Research in southern Africa and the Indian Ocean" (LIA-ARSAIO, contract n. 78682) and PHC-Protea programmes. This work was supported by the French-Argentine ECOS-Sud A16U01 project. We thank E.Quel, L.Otero, P. Artaxo B. Holben, S. Jacobo, S. Piketh, G. Maggs-Kolling, D. Griffith, S. Venkataraman and their staff for establishing and maintaining the Bariloche, Neuquén, Buenos Aires, Sao Paulo, Comodoro, Rio Gallegos, Gobabeb, Pretoria and Durban sites used in this investigation (http://aeronet.gsfc.nasa.gov/). The authors would like to thank the members of the Servicio Meteorologico Nacional (SMN) for their contribution to data acquisition over South America. The authors would like to thank JICA (Japan International Cooperation Agency) and JST (Japan Science and Technology Agency) for the funding support of the SAVER-Net (South American Environmental Risk-Network) network. The MODIS observations used in this paper were produced with the GIOVANNI online data system, developed and maintained by the NASA GES DISC (https://giovanni.gsfc.nasa.gov/giovanni/). We would like to acknowledge the OMI (http://disc.sci.gsfc.nasa.gov/Aura/data-holdings/OMI) and CALIPSO (https//:eosweb.larc.nasa.gov/) programmes for providing access to data via their websites. The authors especially want to thank the staff members of the CEILAP (Centro de Investigaciones en Láseres y Aplicaciones) team working on LiDAR system at the Bariloche site. The authors gratefully acknowledge the NOAA Air Resources Laboratory (ARL) for the provision of the HYSPLIT transport and dispersion model and/or READY website (http://www.ready.noaa.gov) used in this publication.

Data availability

The aerosols optical properties from ground-based (sunphotometer) and satellite (MODIS, CALIOP) observations are available on-line from the sources as stated in the manuscript. The sulfur dioxide measurements from OMI observations are available on-line from the sources as stated in the manuscript. The ***lidar*** data recorded at Bariloche are available from the Servicio Meteorologico Nacional on request.

Author contribution

N.B analysed the sunphotometer measurements and performed the back-trajectory analysis by the use of HYSPLIT model. L.S contributed to MODIS and CALIOP data analysis and interpretation. V.S analysed the sulfur dioxide measurements from OMI observations. J.P contribute to retrieval of aerosol optical properties from LiDAR observations. All authors contributed to data analysis and interpretation. All authors contributed towards the preparation of the paper.

Competing interests

The authors declare that they have no conflicts of interest.

References

Abdou, W. A., Diner, D. J., Martonchik, J. V., Bruegge, C. J., Kahn, R. A., Gaitley, B. J., .Crean., K.A., Remer., L.A. and Holben, B. : Comparison of coincident Multiangle Imaging Spectroradiometer and Moderate Resolution Imaging Spectroradiometer aerosol optical depths over land and ocean scenes containing Aerosol Robotic Network sites. *Journal of Geophysical Research: Atmospheres*, *110*(D10), 2005

Andreae, M. O., Rosenfeld, D., Artaxo, P., Costa, A. A., Frank, G. P., Longo, K. M., and Silva-Dias, M. A. F. D.: Smoking rain clouds over the Amazon. *Science, 303*(5662), 1337-1342, 2004

Alam, K., Qureshi, S., Blaschke, T.: Monitoring spatio-temporal aerosol patterns over Pakistan based on MODIS, TOMS, and MISR satellite data and a HYSPLIT model. *Atmos. Environ.* 45, 4641e4651, 2011

Angström, A.: The parameters of atmospheric turbidity. *Tellus*, 16, 64–75, 1964

Baddock M. C., Bullard J. E., Bryant R. G.: Dust source identification using MODIS: A comparison of techniques applied to the Lake Eyre Basin, Australia. *Remote Sensing of Environment*, 113, 1511–1528. https://doi.org/10.1016/j.rse.2009.03.002, 2009

Baker, A. R., Laskina, O., and Grassian, V. H.: Processing and Ageing in the Atmosphere. In *Mineral dust* (pp. 75-92). *Springer*, Dordrecht, 2014

Bhartia, P. K.: OMI Algorithm Theoretical Basis Document Volume II, OMI Ozone Products, ATBD-OMI-02, Version 2.0, 2002.

Bennouna Y.S., Cachorro V.E., Torres B., Toledano C., Berjón A., de Frutos A.M., Alonso Fernández Coppel I.: Atmospheric turbidity determined by the annual cycle of the aerosol optical depth over north-center Spain from ground (AERONET) and satellite (MODIS), *Atmospheric Environment* 67, 352-364, 2013

Bègue, N., Tulet, P., Chaboureau, J. P., Roberts, G., Gomes, L. and Mallet, M.: Long-range transport of Saharan dust over northwestern Europe during EUCAARI 2008 campaign: Evolution of dust optical properties by scavenging. *Journal of Geophysical Research: Atmospheres*, *117*(D17), 2012

Bègue, N., Vignelles, D., Berthet, G., Portafaix, T., Payen, G., Jégou, F., .Bencherif, H, Jumelet, J., Vernier, J.P., Lurton., T., Renard, J. B., Clarisse., L., Duverger., V., Posny. F., Metzger., J.M. and Godin-Beekmann., S.: Long-range isentropic transport of stratospheric aerosols over

Southern Hemisphere following the Calbuco eruption in April 2015, 10.5194/acp-17-15019-2017, 2017

Bourassa, A. E., Degenstein, D. A., Elash, B. J., and Llewellyn, E. J.: Evolution of the stratospheric aerosol enhancement following the eruptions of Okmok and Kasatochi: Odin-OSIRIS measurements, *Journal of Geophysical Research: Atmospheres*, 115, D00L03,https://doi.org/10.1029/2009JD013274, 2010

Bourassa, A. E., McLinden, C. A., Bathgate, A. F., Elash,B.J., and Degenstein, D. A.: Precision estimate for Odin-OSIRIS limb scatter retrievals, *Journal of Geophysical Research: Atmospheres*, 117, D04303, https://doi.org/10.1029/2011JD016976, 2012

Bréon, F. M., Vermeulen, A. and Descloitres, J.: An evaluation of satellite aerosol products against sunphotometer measurements. *Remote sensing of environment*, *115*(12), 3102-3111, 2011

Carn, S., Clarisse, L., and Prata, A. J.: Multi-decadal satellite measurements of global volcanic degassing, *J. Volcanol. Geotherm.Res*., 311, 99–134, 2016

Chen, B., A. F. Stein, N. Castell, J. D. de la Rosa, A. M. Sanchez de la Campa, Y. Gonzalez-Castanedo, and Draxler, R.R.: Modeling and surface observations of arsenic dispersion from a large Cu-smelter in southwestern Europe. *Atmos. Environ.*, **49**, 114–122, doi:10.1016/j.atmosenv.2011.12.014, 2012

Chu, D. A., Kaufman, Y. J., Ichoku, C., Remer, L. A., Tanré, D. and Holben, B. N.: Validation of MODIS aerosol optical depth retrieval over land. *Geophysical research letters*, *29*(12), MOD2-1, 2002

Clarisse, L., Hurtmans, D., Clerbaux, C., Hadji-Lazaro, J., Ngadi,Y.,and Coheur, P.-F.: Retrieval of sulphur dioxide from the infrared atmospheric sounding interferometer (IASI), *Atmos. Meas. Tech.*, 5, 581–594, https://doi.org/10.5194/amt-5-581-2012, 2012

D'Amico, G., Amodeo, A., Mattis, I., Freudenthaler, V and Pappalardo, G:"EARLINET Single Calculus Chain – technical – Part 1: Pre-processing of raw lidar data". Atmos. Meas. Tech. Discuss., 8, 10387–10428, 2015. www.atmos-meas-tech-discuss.net/8/10387/2015/. doi:10.5194/amtd-8-10387-2015

Das, S., Dey, S., Dash, S. K., Giuliani, G. and Solmon, F.: Dust aerosol feedback on the Indian summer monsoon: Sensitivity to absorption property. *Journal of Geophysical Research: Atmospheres*, *120*(18), 9642-9652, 2015

Deshler, T., Adriani, A., Gobbi, G. P., Hofmann, D. J., Di Donfrancesco, G. and Johnson, B. J.: Volcanic aerosol and ozone depletion within the Antarctic polar vortex during the austral spring of 1991. *Geophysical research letters*, *19*(18), 1819-1822, 1992

Diaz, S. B., Paladini, A. A., Braile, H. G., Dieguez, M. D. C., Deferrari, G. A., Vernet, M., and Vrsalovic, J.: Global and direct UV irradiance variation in the Nahuel Huapi National Park (Patagonia, Argentina) after the eruption of Puyehue-Cordon Caulle (Chile). *Journal of Atmospheric and Solar-Terrestrial Physics*, *112*, 47-56, 2014

Dubovik, O. and King, M. D.: A flexible inversion algorithm for retrieval of aerosol optical properties from Sun and sky radiance measurements. *Journal of Geophysical Research: Atmospheres*, *105*(D16), 20673-20696, 2000

Dubovik, O., Smirnov, A., Holben, B.N., King, M.D., Kaufman., Y.J., Eck., T.F. and Slutsker., I.: Accuracy assessments of aerosol optical properties retrieved from Aerosol Robotic Network (AERONET) sun and sky radiance measurements. *Journal of Geophysical Research: Atmospheres*. 105, 9791-9806, 2000

Dubovik, O., Sinyuk, A., Lapyonok, T., Holben., B.N., Mishchenko, M., Yang., P., Eck., T.F., Volten., H., Muñoz., O., Veihelman., Van der Zande., W.J., Leon., J.F., Sorokin., M. and Slutsker., I.: Application of spheroid models to account for aerosol particle nonsphericity in remote sensing of desert dust. *Journal of Geophysical Research: Atmospheres*. 111, D11208. http://dx.doi.org/10.1029/2005JD006619, 2006

Draxler, R.R., Rolph, G.D.: HYSPLIT (Hybrid Single Particle Lagragian Integrated Trajectory). Air Resources Laborator, National Oceanic and Atmospheric Administration, *Silver Spring*, available at: http://www.arl.noaa.gov/ready/hysplit4.html, 2003

Eck, T.F., Holben, B., Ward, D., Mukelabai, M., Dubovik, O., Smirnov, A., Schafer, J.,Hsu, N., Piketh, S., Queface, A.: Variability of biomass burning aerosol optical characteristics in southern Africa during the SAFARI 2000 dry season campaign and a comparison of single scattering albedo estimates from radiometric measurements. *Journal of Geophysical Research: Atmospheres*. (1984-2012) 108 (D13), 2003

Eck, T.F., Holben, B.N., Dubovik, O., Smirnov, A., Glob, P., Chen, H.B., Chatenet., B., Gomes., L., Zhang., X.Y., Tsay., S.C., Ji., Q., Giles., D. and Slutsker., I.: Columnar aerosol optical properties at AERONET sites in central eastern Asia and aerosol transport to the tropical mid-Pacific. *Journal of Geophysical Research: Atmospheres*. 110 http://dx.doi.org/10.1029/2004JD005274, 2005

El-Metwally M., Alfaro S.C., Abdel Wahab M. M., Zakey A. S., Chatenet B.: Seasonal and inter-annual variability of the aerosol content in Cairo (Egypt) as deduced from the comparison of MODIS aerosol retrievals with direct AERONET measurements. *Atmospheric Research*, 97, 14–25. https://doi.org/10.1016/j.atmosres.2010.03.003, 2010

Fernald, F.G. Analysis of atmospheric lidar observations: some comments. *Appl. Opt.*, 23, 652–653, 1984

Freitas, S. R., Longo, K. M., Silva Dias, M. A. F., Chatfield, R., Silva Dias, P., Artaxo, P., Andreae, M.O., Grell., G., Rodrigues., L.F., Fazenda., A. and Panetta, J.: The coupled aerosol and tracer transport model to the Brazilian developments on the regional atmospheric modeling system (CATT-BRAMS)–Part 1: Model description and evaluation. *Atmospheric Chemistry and Physics*, *9*(8), 2843-2861, 2009

Fioletov, V. E., McLinden, C. A., Krotkov, N., Li, C., Joiner, J., Theys, N., Carn., L. and Moran, M. D.: A global catalogue of large SO2 sources and emissions derived from the Ozone Monitoring Instrument. *Atmospheric Chemistry and Physics*, 16, 11497–11519, 2016

Fyfe, J. C., K. Salzen, J. N. S. Cole, N. P. Gillett, and Vernier., J.P.: Surface response to stratospheric aerosol changes in a coupled atmosphere–ocean model, *Geophysical research letters*, 40, 584–588, doi:10.1002/grl.50156, 2013

Garstang, M., Tyson, P. D., Swap, R., Edwards, M., Kållberg, P. and Lindesay, J. A.: Horizontal and vertical transport of air over southern Africa. *Journal of Geophysical Research: Atmospheres*, *101*(D19), 23721-23736, 1996

Gassmann, M. I., and Mazzeo, N. A.: Air pollution potential: Regional study in Argentina. *Environmental Management*, *25*(4), 375-382, 2000

Guermazi, H., Sellitto, P., Serbaji, M. M., Legras, B. and Rekhiss, F.: Assessment of the Combined Sensitivity of Nadir TIR Aerosols Satellite Observations after a Moderate to Volcanic Stratospheric SO2 and Eruption. *Volcanic Plumes: Impacts on the Atmosphere and Insights into Volcanic Processes*, *7*, 107, 2019

Gooding, J. L., Clanton, U. S., Gabel, E. M. and Warren, J. L.: El Chichón volcanic ash in the stratosphere: particle abundances and size distributions after the 1982 eruption. *Geophysical Research Letters*, *10*(11), 1033-1036, 1983

Hao, W. M., Ward, D. E., Susott, R. A., Babbitt, R. E., Nordgren, B. L., Kaufman, Y. J., .Holben., B.N and Giles, D. M.: Comparison of aerosol optical thickness measurements by

MODIS, AERONET sun photometers, and Forest Service handheld sun photometers in southern Africa during the SAFARI 2000 campaign. *International Journal of Remote Sensing*, *26*(19), 4169-4183, 2005

Hauser, A., Oesch, D. and Foppa, N.: Aerosol optical depth over land: Comparing AERONET, AVHRR and MODIS. *Geophysical research letters*, *32*(17), 2005

Haywood, J. M., A. Jones, and Jones., G.S.: The impact of volcanic eruptions in the period 2000–2013 on global mean temperature trends evaluated in the HadGEM2-ES climate model, *Atmos. Sci. Lett.*, 15(2), 92–96, doi:10.1002/asl2.471, 2013

Hobbs, P.V., J.P. Tuell, D.A. Hegg., L.F. Radke, and Elgroth, M.W.: Particles a nd gases from the 1980-1981 volcanic eruptions of Mr. St. Helens., *Journal of Geophysical Research: Atmosphere*., 87, C12, 11,062-12,086, 1982

Hoelzemann, J. J., Longo, K. M., Fonseca, R. M., Do RosáRio, N. M., Elbern, H., Freitas, S. R., and Pires, C.: Regional representativity of AERONET observation sites during the biomass burning season in South America determined by correlation studies with MODIS Aerosol Optical Depth. *Journal of Geophysical Research: Atmospheres*, *114*(D13), 2009

Ichoku, C., Remer, L. A., and Eck, T. F.: Quantitative evaluation and intercomparison of morning and afternoon Moderate Resolution Imaging Spectroradiometer (MODIS) aerosol measurements from Terra and Aqua. *Journal of Geophysical Research: Atmospheres*, *110*(D10), 2005

Ivy, D. J., Solomon, S., Kinnison, D., Mills, M. J., Schmidt, A., and Neely III, R. R.: The influence of the Calbuco eruption on the 2015 Antarctic ozone hole in a fully coupled chemistry-climate model, *Geophysical research letters*, 44, 2556–2561, https://doi.org/10.1002/2016GL071925, 2017

Jégou, F., Berthet, G., Brogniez, C., Renard, J.-B., François, P.,Haywood, J. M., Jones, A., Bourgeois, Q., Lurton, T., Auriol,F., Godin-Beekmann, S., Guimbaud, C., Krysztofiak, G.,Gaubicher, B., Chartier, M., Clarisse, L., Clerbaux, C., Balois, J.Y., Verwaerde, C., and Daugeron, D.: Stratospheric aerosols from the Sarychev volcano eruption in the 2009 Arctic summer, *Atmospheric Chemistry and Physics*,, 13, 6533–6552, https://doi.org/10.5194/acp-13-6533-2013, 2013.

Kharol S. K., Badarinath K. V. S., Sharma A. R., Kaskaoutis D. G., Kambezidis H. D.: Multiyear analysis of Terra/Aqua MODIS aerosol optical depth and ground observations over tropical urban region of Hyderabad, India. *Atmospheric Environment*, 45, 1532-1542. https://doi.org/10.1016/j.atmosenv.2010.12.047, 2011

Koffman, B. G., Dowd, E. G., Osterberg, E. C., Ferris, D. G., Hartman, L. H., Wheatley, S. D., Kurbatov, A.V., Wong., G.J., Markle., B.R., Dunbar., N.W., Kreutz, K. J. and Yates., M.: Rapid transport of ash and sulfate from the 2011 Puyehue-Cordón Caulle (Chile) eruption to West Antarctica. *Journal of Geophysical Research: Atmospheres*, *122*(16), 8908-8920., 2017

Kravitz, B., Robock, A., and Bourassa, A.: Negligible climatic effects from the 2008 Okmok and Kasatochi volcanic eruptions. *Journal of Geophysical Research: Atmospheres*, 115, D00L05, https://doi.org/10.1029/2009JD013525, 2010

Kravitz, B., Robock, A., Bourassa, A., Deshler, T., Wu, D., Mattis, I., Finger, F., Hoffmann, A., Ritter, C., Bitar, L., Duck, T. J., and Barnes, J. E.: Simulation and observations of stratospheric aerosols from the 2009 Sarychev volcanic eruption, *Journal of Geophysical Research: Atmospheres*, 116, D18211, https://doi.org/10.1029/2010JD015501, 2011

Kristiansen, N. I., Prata, A. J., Stohl, A., and Carn, S. A.: Stratospheric volcanic ash emissions from the 13 February 2014 Kelut eruption, Geophys. Res. Lett., 42, 588–596, https://doi.org/10.1002/2014GL062307, 2015

Krotkov, N.A., McLinden, C.A., Li, C., Lamsal, L.N., Celarier, E.A., Marchenko, S.V., Swartz, W.H., Bucsela, E.J., Joiner, J., Duncan, B.N., Boersma, K.F.: Aura OMI observations of regional SO2 and NO2 pollution changes from 2005 to 2015. *Atmospheric Chemistry and Physics*,, 16 (7), 4605–4629, https://doi.org/10.5194/acp-16-4605-2016, 2016

Kumar, K. R., Kang, N., Sivakumar, V. and Griffith, D.: Temporal characteristics of columnar aerosol optical properties and radiative forcing (2011–2015) measured at AERONET's Pretoria_CSIR_DPSS site in South Africa. *Atmospheric environment*, *165*, 274-289, 2017

Labitzke, K. and McCormick, M.: Stratospheric temperature increases due to Pinatubo aerosols, *Geophysical research letters*, 19, 207–210, 1992

Lehahn, Y., I. Koren, E. Boss, Y. Ben-Ami, and O. Altaratz.: Estimating the maritime component of aerosol optical depth and its dependency on surface wind speed using satellite data, *Atmospheric Chemistry and Physics*,, 10, 6711–6720, doi:10.5194/acp-10-6711-2010, 2010

Li, F., Ginoux, P. and Ramaswamy, V.: Transport of Patagonian dust to Antarctica. *Journal of Geophysical Research: Atmospheres*, *115*(D18), 2010

Li, C., Joiner, J., Krotkov, N.A. and Bhartia, P.K.: A fast and sensitive new satellite SO2 retrieval algorithm based on principal component analysis: application to the ozone monitoring instrument. *Geophysical research letters*, *32*(17). 40 (23), 6314–6318, 2013

Lopes, F.J.S, Mariano, G. L, Landulfo, E and Mariano, E.V.C: Impacts of Biomass Burning in the Atmosphere of the Southeastern Region of Brazil Using Remote Sensing Systems, Atmospheric Aerosols - Regional Characteristics - Chemistry and Physics, Hayder Abdul-Razzak, IntechOpen, DOI: 10.5772/50406 : https://www.intechopen.com/books/atmospheric-aerosols-regional-characteristicschemistry-and-physics/impacts-of-biomass-burning-in-the-atmosphere-of-thesoutheastern-region-of-brazil-using-remote-sensi, 2012

***J. S. Lopes, F.; Silva, J.J.; Antuña Marrero, J.C.; Taha, G and Landulfo, E. Synergetic Aerosol Layer Observation after the 2015 Calbuco Volcanic Eruption Event. Remote Sens. 2019, 11, 195*.**

Madry, W. L.,O. B. Toon, and O'Dowd., C.D.: Modeled optical thickness of sea-salt aerosol, *Journal of Geophysical Research: Atmospheres*, 116, D08211, doi:10.1029/2010JD014691, 2011

Mather, T.A.; Tsanev, V.I.; Pyle, D.M.; McGonigle, A.J.S.; Oppenheimer, C.; Allen, A.G.: Characterization and evolution of tropospheric plumes from Lascar and Villarrica volcanoes, Chile. *Journal of Geophysical Research: Atmospheres*, 109, D21303, 2004

Martin, R.S.; Mather, T.A.; Pyle, D.M.; Power, M.; Tsanev, V.I.; Oppenheimer, C.; Allen, A.G.; Horwell, C.J. and Ward, E.P.W.: Size distributions of fine silicate and other particles in Masaya's volcanic plume. *Journal of Geophysical Research: Atmospheres*, 114, D09217, 2009

McCormick, M. P., Thomason, L. W., and Trepte, C. R.: Atmospheric effects of the Mt Pinatubo eruption, *Nature*, 373, 399–404, 1995

More, S., Kumar, P.P., Gupta, P., Devara, P.C.S., Aher, G.: Comparison of aerosol products retrieved from AERONET, MICROTOPS, and MODIS over a tropical urban city, Pune, India. *Aerosol Air Qual. Res*. 13, 107e121, 2013

Mills, M. J., Schmidt, A., Easter, R., Solomon, S., Kinnison, D. E., Ghan, S. J., Neely III., R. R., Marsh., D. R., Conley., A., Bardeen., C.G. and Gettelman., A. : Global volcanic aerosol properties derived from emissions, 1990–2014, using CESM1 (WACCM). *Journal of*

Geophysical Research: Atmospheres, *121*, 2332–2348. https://doi.org/10.1002/2015JD024290, 2016

Neely III, R. R., Toon., O.B., Solomon.,S., Vernier., J.P., Alvarez., C., English., E.M., Rosenlof., K. H., Mills., J. M., Bardeen., C.G., Daniel., J. S. and Thayer., J. P.: Recent anthropogenic increases in SO2 from Asia have minimal impact on stratospheric aerosol, *Geophysical research letters*, *32*(17), 40, 999–1004, doi:10.1002/grl.50263, 2013

Ningombam, S. S., Larson, E. J. L., Dumka, U. C., Estellés, V., Campanelli, M., and Steve, C.: Long-term (1995–2018) aerosol optical depth derived using ground based AERONET and SKYNET measurements from aerosol aged-background sites. *Atmospheric Pollution Research*, *10*(2), 608-620, 2019

Omar, M.A, Hu, A.H, Powell,.Y, Liu, K.A, Hunt,. Z., Young, .W.H.: Overview of the CALIPSO Mission and CALIOP Data Processing Algorithms. *Journal of Atmospheric and Oceanic Technology*, 26, 2310–2323, 2009

Otero, L. A., Ristori, P. R., Papandrea, S. D., Pallotta, J. V., D'elia, R. L. and Quel, E. J.: Mediciones en la patagonia argentina de espesor óptico de aerosoles con fotómetros solares de la red AERONET, *Asociación Física Argentina; Anales AFA*; 26; 4; 12-2015; 186-189, 2015

Piketh, S. J., Annegarn, H. J. and Tyson, P. D.: Lower tropospheric aerosol loadings over South Africa: The relative contribution of aeolian dust, industrial emissions, and biomass burning. *Journal of Geophysical Research: Atmospheres*, *104*(D1), 1597-1607, 1999

Porter, J.N.; Horton, K.A.; Mouginis-Mark, P.J.; Lienert, B.; Sharma, S.K.; Lau, E.; Sutton, A.J.; Elias, T. and Oppenheimer, C.: Sun photometer and lidar measurements of the plume from the Hawaii Kilauea Volcano Pu'u O'o vent: Aerosol flux and SO2 lifetime. *Geophysical research letters*, *32*(17), 29, 30-1–30-4, 2002

Prasad, A.K. and Singh, R.P.: Comparison of MISR-MODIS aerosol optical depth over the Indo-Gangetic basin during the winter and summer seasons (2000e2005). *Remote Sens. Environ*. 107, 109e119, 2007

Reckziegel, F., Bustos, E., Mingari, L., Báez, W., Villarosa, G., Folch, A., Collini., E., Viramonte., J., Romero., J. and Osores, S.: Forecasting volcanic ash dispersal and coeval resuspension during the April–May 2015 Calbuco eruption. *Journal of Volcanology and Geothermal Research*, *321*, 44-57, 2016

Ridley, D. A., et al. : Total volcanic stratospheric aerosol optical depths and implications for global climate change, Geophys. Res. Lett., 41(22), 7763-7769, doi:10.1002/2014GL061541, 2014

Ristori., P., Otero, L., Jin., Y., Barja., B., Shimizu., A., Barbero., A., Salvador., J. Bali., J.L., Herrera., M., Etala., P., Acquesta., A., Quel., E. Sugimoto., N. and Mizuno.: A. SAVER.NET LiDAR network in Southern America. *EPJ Web of Conferences* 176, 09011. https://doi.org/10.1051/epjconf/201817609011, 2018

Rose, W.I., R.L. Chaun, and D.C. Woods, Small particles in the plume of Mr. St. Helens, *Journal of Geophysical Research: Atmospheres*, 87, C7, 4956-4962, 1982.

Rose, W. I., Bluth, G. J. S. and Ernst, G. G.: Integrating retrievals of volcanic cloud characteristics from satellite remote sensors: a summary. *Philosophical Transactions of the Royal Society of London. Series A: Mathematical, Physical and Engineering Sciences*, *358*(1770), 1585-1606, 2000

Sakai, T., Uchino, O., Nagai, T., Liley, B., Morino, I. and Fujimoto, T: Long-term variation of stratospheric aerosols observed with lidars over Tsukuba, Japan, from 1982 and Lauder, New Zealand, from 1992 to 2015. Journal of Geophysical Research: Atmospheres, 121(17), 10-283, 2016

Sangeetha, S. K., Sivakumar, V. and Gebreslasie, M.: Long-range transport of SO2 over South Africa: A case study of the Calbuco volcanic eruption in April 2015. *Atmospheric Environment*, *185*, 78-90, 2018

Sawamura, P., Vernier, J. P., Barnes, J. E., Berkoff, T. A., Welton, E. J., Alados-Arboledas, L., and Lange, D.: Stratospheric AOD after the 2011 eruption of Nabro volcano measured by lidars over the Northern Hemisphere, *Environ. Res. Lett.*, 7, 034013, https://doi.org/10.1088/1748-9326/7/3/034013, 2012, 2012

Sellitto, P.; Salerno, G.; La Spina, A.; Caltabiano, T.; Terray, L.; Gauthier, P.J. and Briole, P.: A novel methodology to determine volcanic aerosols optical properties in the UV and NIR and Ångström parameters using Sun photometry. J. Geophys. Res. Atmos., 122, 9803–9815, 2017

Sellitto, P., Spampinato, L., Salerno, G. and La Spina, A.: Aerosol Optical Properties of Pacaya Volcano Plume Measured with a Portable Sun-Photometer. *Geosciences*, *8*(2), 36, 2018

Shikwambana, L. and Sivakumar, V.: Long-range transport of volcanic aerosols over South Africa: a case study of the Calbuco volcano eruption in Chile during April 2015. *South. African. Geographical. Journal*., https://doi.org/10.1080/03736245.2018.1498383, 2018

Shaw,G .E.: Sun photometry. Bull. Am. Meteorol. Soc. 64, 1, 4-10, 1983

Stein, A. F., Draxler, R. R., Rolph, G. D., Stunder, B. J. B., Cohen, M. D. and Ngan, F.: NOAA's HYSPLIT atmospheric transport and dispersion modeling system. *Bulletin of the American Meteorological Society*, 96, 2059–2077, 2015

Shi, Y., Zhang, J., Reid, J. S., Holben, B., Hyer, E. J. and Curtis, C.: An analysis of the collection 5 MODIS over-ocean aerosol optical depth product for its implication in aerosol assimilation. *Atmospheric Chemistry and Physics*, *11*(2), 557-565, 2011

Solomon, S., Portmann, R. W., Garcia, R. R., Thomason, L. W.,Poole, L. R., and McCormick, M. P.: The role of aerosol variations in anthropogenic ozone depletion at northern midlatitudes, *Journal of Geophysical Research: Atmospheres*, 101, 6713–6727, 1996

Solomon, S.: Stratospheric ozone depletion.: A review of concepts and history, *Rev. Geophys.*, 37, 275–316,https://doi.org/10.1029/1999RG900008, 1999

Solomon, S., Portmann, R. W., Sasaki, T., Hofmann, D. J., & Thompson, D. W. J.: Four decades of ozonesonde measurements over Antarctica. *Journal of Geophysical Research: Atmospheres, 110*, D21311. https://doi.org/10.1029/2005JD005917, 2005

Solomon, S., Daniel, J. S., Neely III, R. R., Vernier, J.-P., Dutton, E. G., and Thomason, L. W.: The persistently variable "Background"stratospheric aerosol layer and global climate change, Science 333, 866–870, https://doi.org/10.1126/science.1206027, 2011

Solomon, S., Ivy, D. J., Kinnison, D., Mills, M. J., Neely III, R. R., and Schmidt A.: Emergence of healing in the Antarctic ozone layer, Science, 252, 269–274, https://doi.org/10.1126/science.aae0061, 2016

Stone, K. A., Solomon, S., Kinnison, D. E., Pitts, M. C., Poole, L. R., Mills, M. J., Schmidt., A., Neely III, R. R., Ivy., D., Schwartz., M. J., Vernier., J.P., Johnson., B. J., Tully., M. B., Klekocius., A. R., König-Langlo., G., and Hagiya., S.: Observing the impact of Calbuco volcanic aerosols on south polar ozone depletion in 2015. *Journal of Geophysical Research: Atmospheres*, *122*, 11,862–11,879. https://doi.org/10.1002/2017JD026987, 2017

Stunder., B. J. B., Heffter, J. L. and Draxler, R.R.: Airborne volcanic ash forecast area reliability. *Weather. Forecasting*, **22**, 1132–1139, doi:10.1175/WAF1042.1, 2007

Sparks, R. S. J., M. I. Bursik, S. N. Carey, J. S. Gilbert, L. S. Glaze, H. Sigurdsson, and Woods., A.W.: Volcanic Plumes, *John Wiley*, Chichester, U. K, 1997

Tie, X., and Brasseur, G.: The response of stratospheric ozone to volcanic eruptions: Sensitivity to atmospheric chlorine loading. *Geophysical Research Letters*, *22*(22), 3035–3038. https://doi.org/10.1029/95GL03057, 1995

Theys,N.,DeSmedt,I.,VanRoozendael,M.,Froidevaux,L.,Clarisse,L., and Hendrick,F.: First satellite detection of volcanic OClO after the eruption of Puyehue-Cordón Caulle, *Geophysical Research Letters*, 41, 667–672, doi:10.1002/2013GL058416, 2014. 23643, 2013

Toth, T. D., Zhang, J., Campbell, J. R., Reid, J. S., Shi, Y., Johnson, R. S., Sirmonv., A., Vaughan., M. A. and Winker, D. M.: Investigating enhanced Aqua MODIS aerosol optical depth retrievals over the mid-to-high latitude Southern Oceans through intercomparison with co-located CALIOP, MAN, and AERONET data sets. *Journal of Geophysical Research: Atmospheres*, *118*(10), 4700-4714, 2013

Torres, O., Chen, Z., Jethva, H., Ahn, C., Freitas, S. R. and Bhartia, P. K.: OMI and MODIS observations of the anomalous 2008–2009 Southern Hemisphere biomass burning seasons. *Atmospheric Chemistry and Physics*, *10*(8), 3505-3513, 2010

Trickl, T., Giehl, H., Jäger, H., and Vogelmann, H.: 35 yr of stratospheric aerosol measurements at Garmisch-Partenkirchen: from Fuego to Eyjafjallajökull, and beyond, *Atmospheric Chemistry and Physics*, 13, 5205–5225, https://doi.org/10.5194/acp-13-5205-2013, 2013

Tripathi, S.N., Dey, S., Chandel, A., Srivastava, S., Singh, R.P., Holben, B.N.: Comparison of MODIS and AERONET derived aerosol optical depth over the Ganga Basin, India. *Ann. Geophys.* 23, 1093e1101, 2005

Thomason, L.W., Pitts, M. C., and Winker, D. M.: CALIPSO observations of stratospheric aerosols: a preliminary assessment, *Atmospheric Chemistry and Physics*, 7, 5283–5290, https://doi.org/10.5194/acp-7-5283-2007, 2007

Tomasi.,C., Vitale., V and Tarrozi., L.: Sun-photometric measurements of atmospheric turbidity variation a used by the Pinatubo aerosol cloud in the Himalayan region during the summer periods of 1991 and 1992. *Nouvo Cimento*, 20C, 1, 61-88, 1997

Vanhellemont, F., D. Fussen, N. Mateshvili, C. Tétard, C. Bingen, E. Dekemper, N. Loodts, E. Kyrölä, V. Sofieva, and Tamminen, J.: Optical extinction by upper tropospheric/stratospheric aerosols and clouds: GOMOS observations for the period 2002–2008, *Atmospheric Chemistry and Physics.*, *10*, 7997–8009, 2010

Vermote, E. F., El Saleous, N., Justice, C. O., Kaufman, Y. J., Privette, J. L., Remer, L., .Roger., J.C. and Tanre, D.: Atmospheric correction of visible to middle-infrared EOS-MODIS data over land surfaces: Background, operational algorithm and validation. *Journal of Geophysical Research: Atmospheres*, *102*(D14), 17131-17141, 1997

Vernier, J.-P., Thomason, L. W., Pommereau, J.-P., Bourassa, A.,Pelon, J., Garnier, A., Hauchecorne, A., Blanot, L., Trepte,C., Degenstein, D., and Vargas, F.: Major influence of tropical volcanic eruptions on the stratospheric aerosol layer during the last decade, *Geophysical Research Letters*, 38, L12807, https://doi.org/10.1029/2011GL047563, 2011

Vernier, J. P., Fairlie, T. D., Deshler, T., Natarajan, M., Knepp, T., Foster, K., Weinhold., F.G., Bedka., K.M., Thomason., L. and Trepte, C.: In situ and space-based observations of the Kelud volcanic plume: The persistence of ash in the lower stratosphere. *Journal of Geophysical Research: Atmospheres*, *121*(18), 11-104, 2016

Watson, I. M., Oppenheimer, C., Voight, B., Francis, P. W., Clarke, A., Stix, J., Miller., A., Pyle., D.M., Burton., M.R., Young., S.R., Norton., G., Loughlin., S., Darroux., B. and Staff., M.V.O.: The relationship between degassing and ground deformation at Soufriere Hills Volcano, Montserrat. *Journal of Volcanology and Geothermal Research*, *98*(1-4), 117-126, 2000

Watson, I.M. and Oppenheimer, C.: Photometric observations of Mt. Etna's different aerosol plumes. *Atmos. Environ.*, 35, 3561–3572, 2001

Webster, H. N., Thomson, D. J., Johnson, B. T., Heard, I. P. C., Turnbull, K., Marenco, F., Kristiansen., N.I., Dorsey., J., Minikin., A., Weinzierl, B., Schumann, U., Sparks, R.S.J., Loughlin, S.C., Hort, M.C., Leadbetter, S.J., Devenish, B.J., A. J. Manning, A.J., Witham, C.S, Haywood, J.M., and Golding., B.W.: Operational prediction of ash concentrations in the distal volcanic cloud from the 2010 Eyjafjallajökull eruption. *Journal of Geophysical Research: Atmospheres*, *117*(D20), 2012

Winker, D.M., Vaughan, Angström, A.: The parameters of atmospheric turbidity. *Tellus*, 16, 64–75, 1964

Winker D. M., Pelon J., Coakley Jr. J. A., Ackerman S. A., Charlson R. J., Colarco P. R., Wielicki B. A.: The CALIPSO Mission: A Global 3D View of Aerosols and Clouds, *Bulletin of the American Meteorological Society* doi:10.1175/2010BAMS3009.1, 2010

Winker D. M., Tackett J. L., Getzewich B. J., Liu Z., Vaughan M. A., Rogers R. R.: The global 3-D distribution of tropospheric aerosols as characterized by CALIOP, *Atmospheric Chemistry and Physics*, 13, 3345–3361. doi:10.5194/acp-13-3345-2013, 2013

Young, R., Houben, H., and Toon, O.: Radiatively forced dispersion of the Mt. Pinatubo volcanic cloud and induced temperature perturbation in the stratosphere during the first few months following the eruption, *Geophysical Research Letters*, 21, 369–372, 1994

Zhang, J., and Reid, J. S.: MODIS aerosol product analysis for data assimilation: Assessment of over-ocean level 2 aerosol optical thickness retrievals. *Journal of Geophysical Research: Atmospheres*, *111*(D22), 2006

Zhu, Y., Toon, O. B., Kinnison, D., Harvey, V. L., Mills, M. J., Bardeen, C. G., Pitts., M., Bègue., N., Renard., J.B., Berthet., G. and Jégou, F.: Stratospheric Aerosols, Polar Stratospheric Clouds, and Polar Ozone Depletion After the Mount Calbuco Eruption in 2015. *Journal of Geophysical Research: Atmospheres*, *123*(21), 12-308, 2018

Zuev, V. V., Savelieva, E. S., and Parezheva, T. V.: Study of the Possible Impact of the Calbuco Volcano Eruption on the Abnormal Destruction of Stratospheric Ozone over the Antarctic in Spring 2015. *Atmospheric and Oceanic Optics*, *31*(6), 665-669, 2018

FIGURES AND TABLES

Site	Instruments	Period	Daily observation	Background
Gobabeb	Sunphotometer	2014-2016	694	407
(23°S-15°E)	MODIS	2002-2016	2469	1954
Sao Paulo	Sunphotometer	2000-2016	1957	1676
(23°-46°W)	MODIS	2002-2016	2884	2369
Pretoria	Sunphotometer	2011-2015	1222	905
(25°S-28°E)	MODIS	2002-2016	3432	2281
Durban	Sunphotometer	2015-2016	232	89
(29°S-31°E)	MODIS	2002-2016	3731	3216
Buenos Aires	Sunphotometer	1999-2016	3237	2374
(34°S-58°W)	MODIS	2002-2016	3163	2648
Neuquen	Sunphotometer	2013-2016	678	407
(38°S-68°W)	MODIS	2002-2016	3495	2980
Bariloche	Sunphotometer	2012-2016	463	229
(41°S-71°W)	MODIS	2002-2016	2321	1806
Comodoro	Sunphotometer	2013-2016	830	546
(45°S-67°W)	MODIS	2002-2016	3495	2980
Rio Gallegos	Sunphotometer	2009-2016	1245	1000
(51°S-69°W)	MODIS	2002-2016	1204	689

Table 1. Number of available and background daily observations at each site for both sunphotometer and MODIS.

Site	Sunphotometer		MODIS	
	Duration of stay	**Anomaly (%)**	**Duration of stay**	**Anomaly (%)**
Gobabeb	01/05 - 04/05	22.5 ±13.0 %	01/05 - 06/05	20.1 ± 11.2 %
Sao Paulo	27/04 - 02/05	44.5 ± 24.5 %	26/04 - 01/05	43.4 ± 19.4 %
Pretoria	06/05 - 08/05	14.6 ± 5.7 %	02/05 - 07/05	20.7 ± 11.2 %
Durban	04/05 – 08/05	24.8 ± 11.1 %	03/05 - 07/05	27.5 ± 10.8 %
Buenos Aires	27/05 – 01/05	30.6 ± 5.6 %	24/05 – 03/05	35.5 ± 2.8 %
Neuquen	29/04	40.3 ± 0 %	23/04 – 07/05	37.2 ± 15.2 %
Bariloche	24/04 – 25/04	53.6 ± 45.1 %	23/04 – 10/05	60.2 ± 30.6 %
Comodoro	29/04 – 30/04	26.4 ± 1.5 %	26/04 – 2/05	14.5 ± 2.5 %

Table 2. Averaged anomaly of AOD and corresponding standard deviation (in percentage) induced by the Calbuco plume during its duration of stay over each site.

Site	Latitude [°]	R^2	MBE (%) $\frac{1}{n}\sum_{i=1}^{n}\frac{Phot_i - Mod_i}{Phot_i}$	RMSE (%) $\sqrt{\frac{1}{n-1}\sum_{i=1}^{n}(Phot_i - Mod_i)^2}$
Gobabeb	-23°	0.69	8.2 ± 0.9	8.2
Sao Paulo	-23°	0.70	5.2 ± 1.8	4.6
Pretoria	-25°	0.76	4.7 ± 1.7	8.7
Durban	-29°	0.71	6.9 ± 2.1	6.1
Buenos Aires	-34°	0.68	-7.1 ± 1.5	4.2
Neuquén	-38°	0.63	-8.7 ± 2.9	7.4
Bariloche	-41°	0.64	-7.6 ± 3.3	6.3
Comodoro	-45°	0.51	- 9.7 ± 3.2	13.2
Rio Gallegos	-51°	0.59	-8.1 ± 4.2	10.4

Table 3. Statistical parameter for the comparison between Sunphotometer *(Phot)* and MODIS *(Mod)* observations for each site.

	Bariloche		Neuquén		Buenos Aires		Sao Paulo	
	α_P	β_P	α_P	β_P	α_P	β_P	α_P	β_P
24th April	-0.01 (±0.02)	0.16 (±0.02)						
25th April	0.02 (±0.05)	0.19 (±0.02)						
26th April								
27th April					1.6 (±0.6)	0,01 (±0.06)	1.3 (±0.2)	0.04 (±0.03)
28th April					0,8 (±0,3)	0.01 (±0.005)	1.1 (±0.4)	0.04 (±0.02)
29th April			1.4 (±0.1)	0.04 (±0.02)			1.2 (±0.2)	0.02 (±0.6
30th April					0.87 (±0.09)	0.05 (±0.006)		

Table 4. Mean and standard deviation for the plume-isolated Angström exponent and turbidity during the 24th-30th April for the Bariloche, Neuquén, Buenos Aires and Sao Paulo. These values are obtained from sunphotometer measurements. The grey grids indicate that there were no observations.

	Gobabeb		Pretoria		Durban	
	α_P	β_P	α_P	β_P	α_P	β_P
01st May	0.35 (±0.9)	0.03 (±0.007)				
02nd May	0.42 (±0.06)	0.16 (±0.006)				
03rd May	1.1 (±0.75)	0.06 (±0.005)				
04th May	0.87 (±0.11)	0.01 (±0.008)			0.55 (±0.14)	0.05 (±0.02)
05th May					0.72 (±0.36)	0.02 (±0.006)
06th May			1.5 (±0.41)	0.004 (±0.002)	1.1 (±0.30)	0.04 (±0.005)
07th May			1.2 (±0.40)	0.02 (±0.01)	1.85 (±0.85)	0.014 (±0.012)
08thMay			0.5 (±0.30)	0.09 (±0.01)	1.18 (±0.23)	0.02 (±0.01)

Table 5. Mean and standard deviation for the plume-isolated Angström exponent and turbidity during the 01st-08th May for the Gobabeb, Pretoria and Durban. The grey grids indaicate that there were no observations.

1

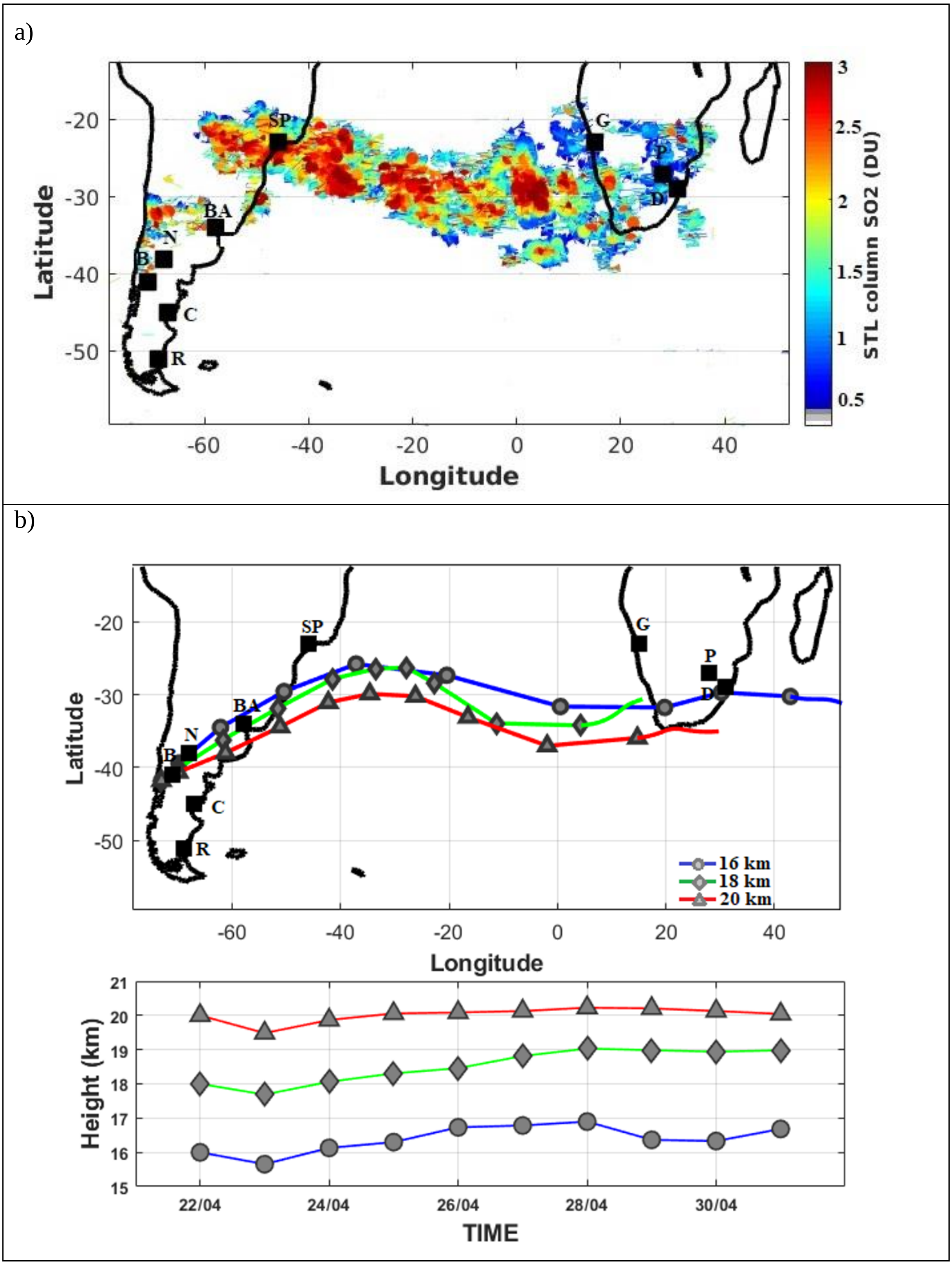

a)
SP
G
P
D
BA
N
B
C
R
Latitude
Longitude
STL column SO2 (DU)
b)
16 km
18 km
20 km
Latitude
Longitude
Height (km)
TIME
22/04
24/04
26/04
28/04
30/04

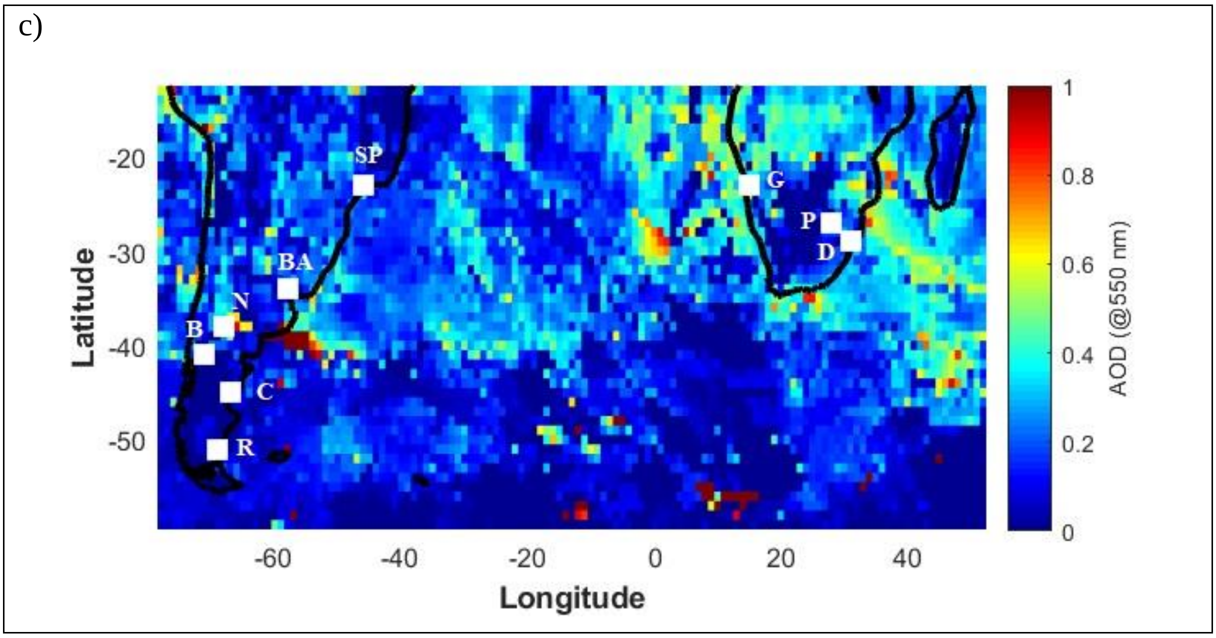

Figure 1: (a) Time averaged map of SO_2 column in the lower stratosphere observed by OMI during the 22 April-1 May period. (b) Forward-trajectories analysis of air masses from HYSPLIT model starting at the Calbuco volcano coordinates at 16 km (blue line with grey dots), 18 km (green line with grey diamonds) and 20 km (red line with grey triangles). (c) Time averaged map of MODIS AOD (550 nm) during the 22 April-1 May period. The localization of the selected sites are indicated by black boxes and their initials: (B) Bariloche, (N) Neuquén, (BA) Buenos Aires, (SP) Sao Paulo, (C) Comodoro, (R) Rio Gallegos, (G) Gobabeb, (D) Durban, (P) Pretoria.

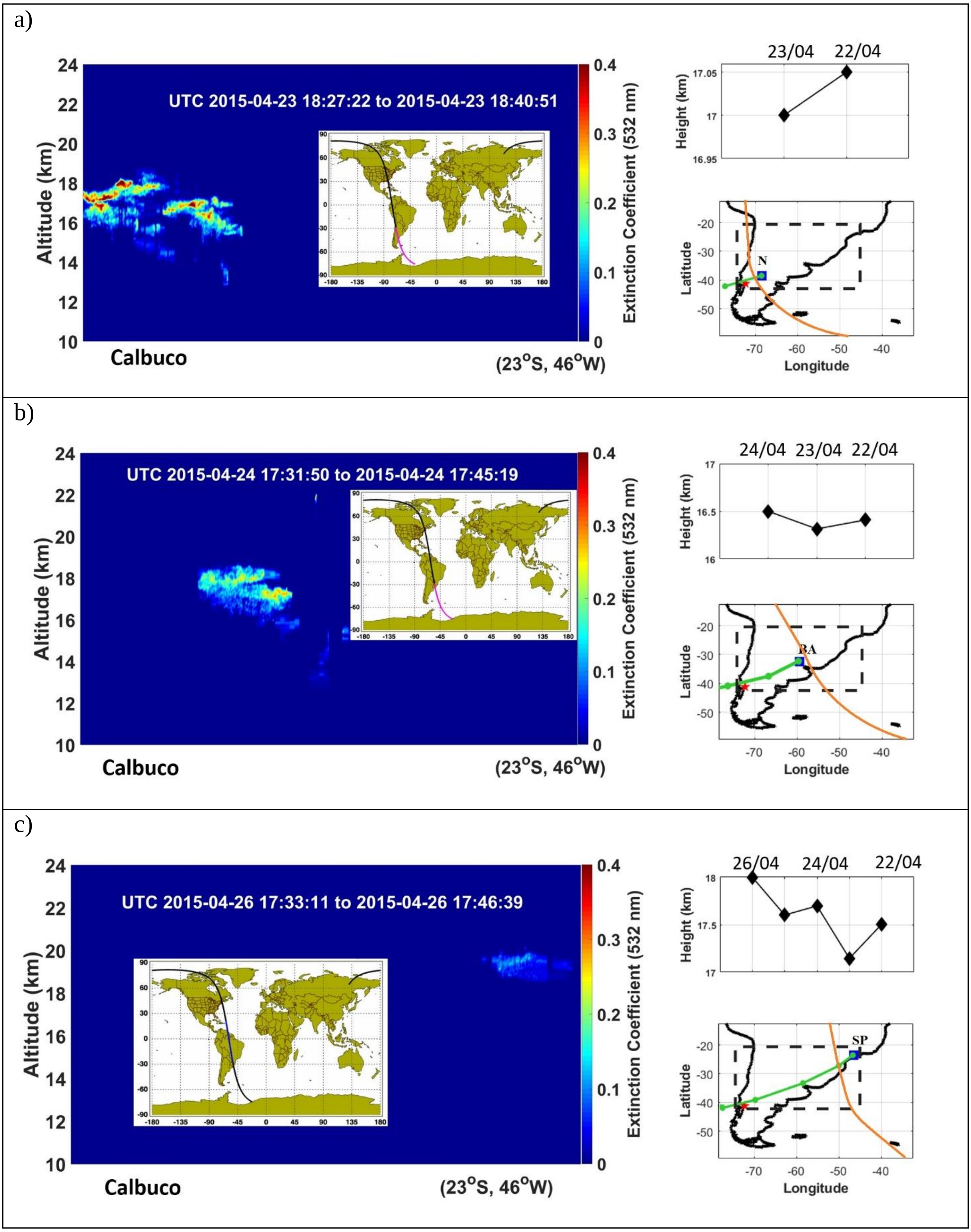

Figure 2: Daily zonal extinction coefficient (km^{-1}) at 532 nm observed by CALIOP over the Calbuco volcano and in the vicinity of the Sao Paulo site (23˚S, 46˚W) on (a) 23 April, (b) 24 April and (c) 26th April. The red star and the blue square correspond to the localization of the Calbuco volcano and the maximum extinction values respectively. Back-trajectory analysis between the maximum extinction values and the Calbuco volcano are plotted by the green curve. The CALIPSO overpass trajectories are plotted by the orange curve.

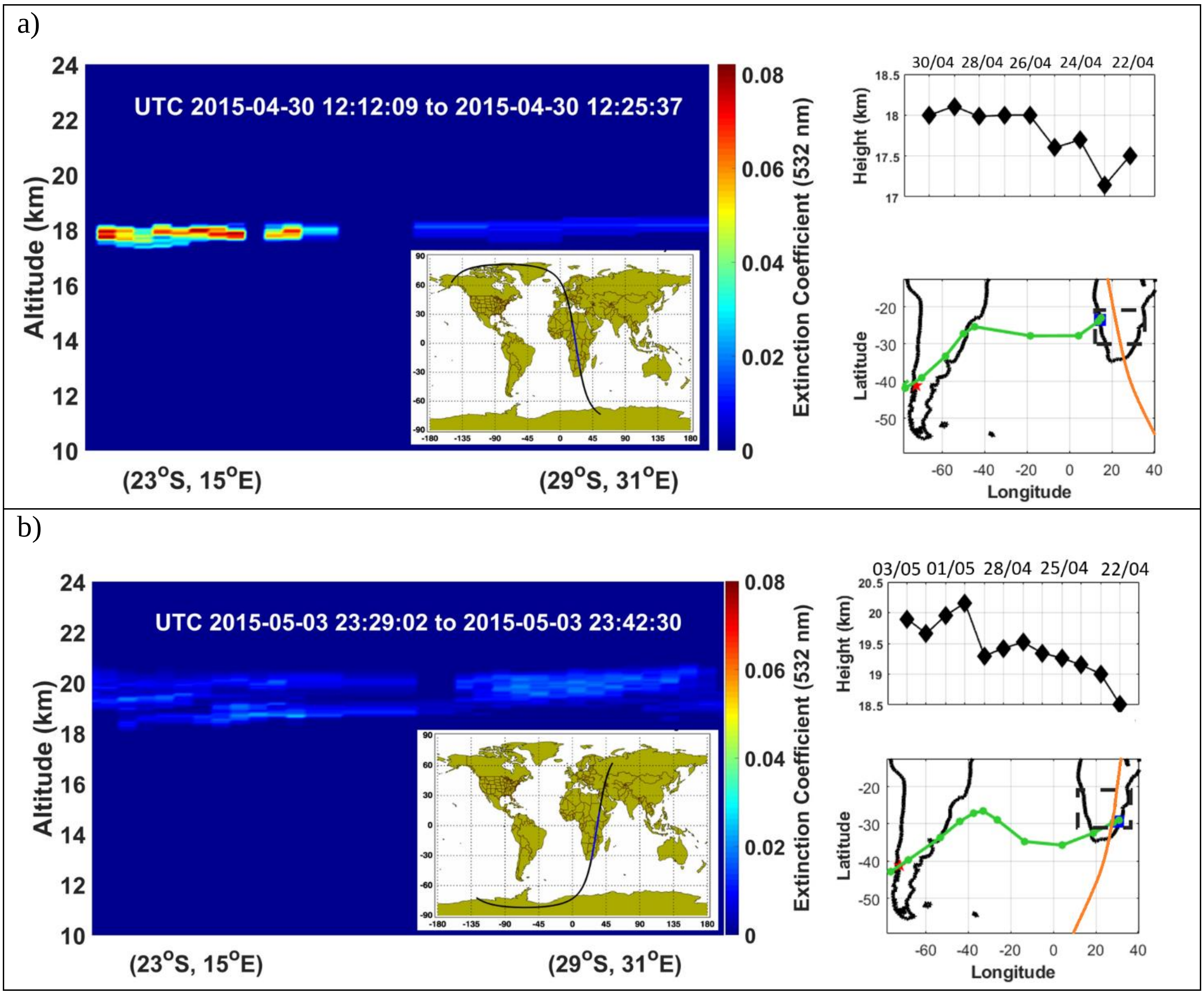

Figure 3: Daily zonal extinction coefficient (km^{-1}) at 532 nm observed by CALIOP over the South African region on (a) 30 April and (b) 3 May. The red star and the blue square correspond to the localization of the Calbuco volcano and the maximum extinction values respectively. Back-trajectory analysis between the maximum extinction values and the Calbuco volcano is represented by the green curve.

1

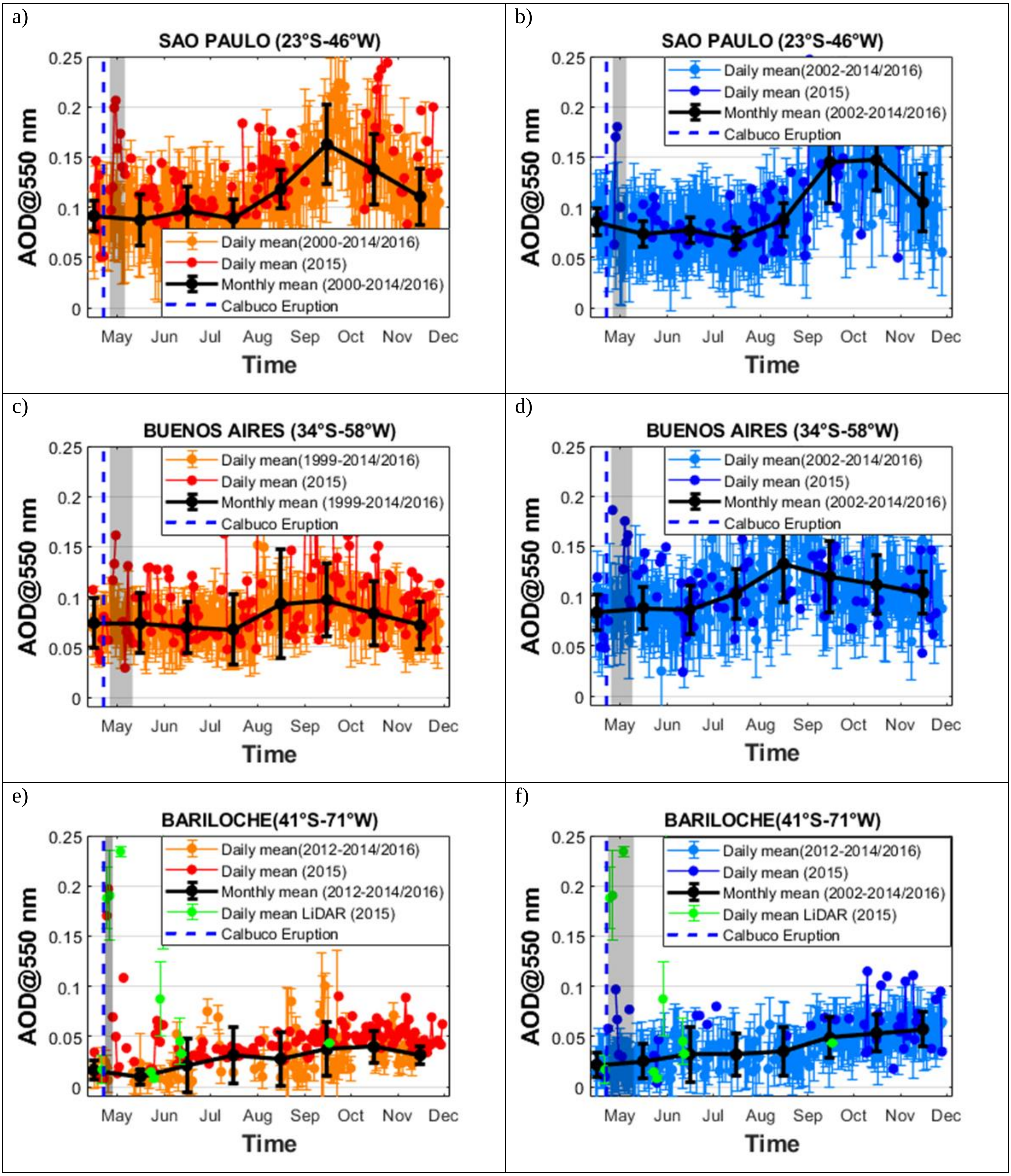

a)
SAO PAULO (23°S-46°W)
Daily mean(2000-2014/2016)
Daily mean (2015)
Monthly mean (2000-2014/2016)
Calbuco Eruption
AOD@550 nm
Time
b)
SAO PAULO (23°S-46°W)
Daily mean(2002-2014/2016)
Daily mean (2015)
Monthly mean (2002-2014/2016)
Calbuco Eruption
c)
BUENOS AIRES (34°S-58°W)
Daily mean(1999-2014/2016)
Daily mean (2015)
Monthly mean (1999-2014/2016)
Calbuco Eruption
d)
BUENOS AIRES (34°S-58°W)
Daily mean(2002-2014/2016)
Daily mean (2015)
Monthly mean (2002-2014/2016)
Calbuco Eruption
e)
BARILOCHE(41°S-71°W)
Daily mean(2012-2014/2016)
Daily mean (2015)
Monthly mean (2012-2014/2016)
Daily mean LiDAR (2015)
Calbuco Eruption
f)
BARILOCHE(41°S-71°W)
Daily mean(2012-2014/2016)
Daily mean (2015)
Monthly mean (2002-2014/2016)
Daily mean LiDAR (2015)
Calbuco Eruption
May Jun Jul Aug Sep Oct Nov Dec

Figure 4: Daily mean of AOD (550 nm) obtained over (a,b) Sao Paulo, (c,d) Buenos Aires and (e,f) Bariloche obtained from Sunphotometer and LiDAR (on the left panel) and from MODIS observations (on the right panel) from 15 April to 1 December. The grey area corresponds to the influence of the volcanic plume over a given site. The black line indicates the monthly mean values.

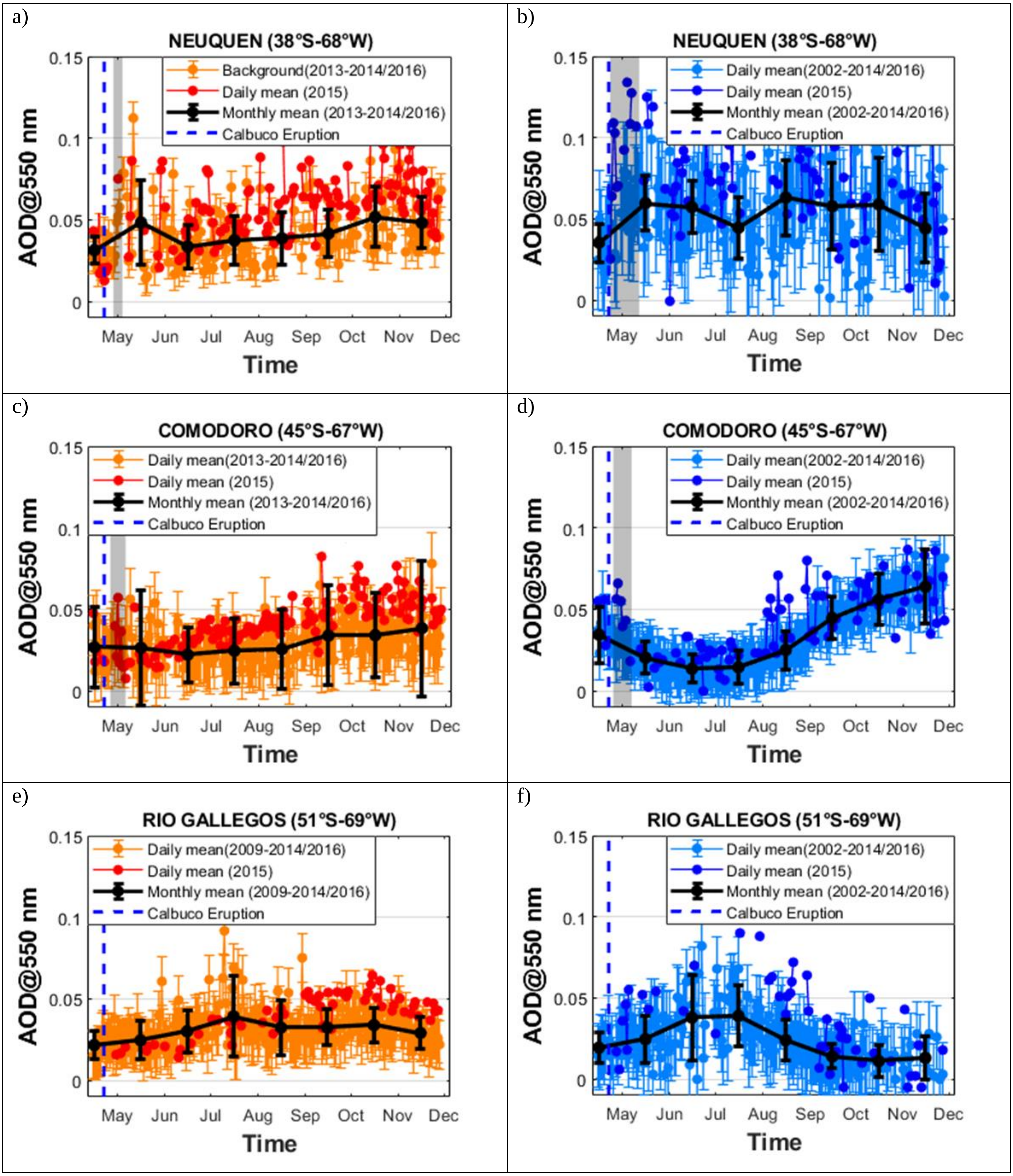
a)
NEUQUEN (38°S-68°W)
Background(2013-2014/2016)
Daily mean (2015)
Monthly mean (2013-2014/2016)
Calbuco Eruption
AOD@550 nm
0.15
0.1
0.05
0
May Jun Jul Aug Sep Oct Nov Dec
Time
b)
NEUQUEN (38°S-68°W)
Daily mean(2002-2014/2016)
Daily mean (2015)
Monthly mean (2002-2014/2016)
Calbuco Eruption
AOD@550 nm
0.15
0.1
0.05
0
May Jun Jul Aug Sep Oct Nov Dec
Time
c)
COMODORO (45°S-67°W)
Daily mean(2013-2014/2016)
Daily mean (2015)
Monthly mean (2013-2014/2016)
Calbuco Eruption
AOD@550 nm
0.15
0.1
0.05
0
May Jun Jul Aug Sep Oct Nov Dec
Time
d)
COMODORO (45°S-67°W)
Daily mean(2002-2014/2016)
Daily mean (2015)
Monthly mean (2002-2014/2016)
Calbuco Eruption
AOD@550 nm
0.15
0.1
0.05
0
May Jun Jul Aug Sep Oct Nov Dec
Time
e)
RIO GALLEGOS (51°S-69°W)
Daily mean(2009-2014/2016)
Daily mean (2015)
Monthly mean (2009-2014/2016)
Calbuco Eruption
AOD@550 nm
0.15
0.1
0.05
0
May Jun Jul Aug Sep Oct Nov Dec
Time
f)
RIO GALLEGOS (51°S-69°W)
Daily mean(2002-2014/2016)
Daily mean (2015)
Monthly mean (2002-2014/2016)
Calbuco Eruption
AOD@550 nm
0.15
0.1
0.05
0
May Jun Jul Aug Sep Oct Nov Dec
Time

Figure 5: Daily mean of AOD (550 nm) obtained over (a,b) Neuquén, (c,d) Comodoro and (e,f) Rio Gallegos obtained from Sunphotometer (on the left panel) and from MODIS observations (on the right panel) from 15 April to 1 December. The grey area corresponds to the influence of the volcanic plume over a given site. The black line indicates the monthly mean values.

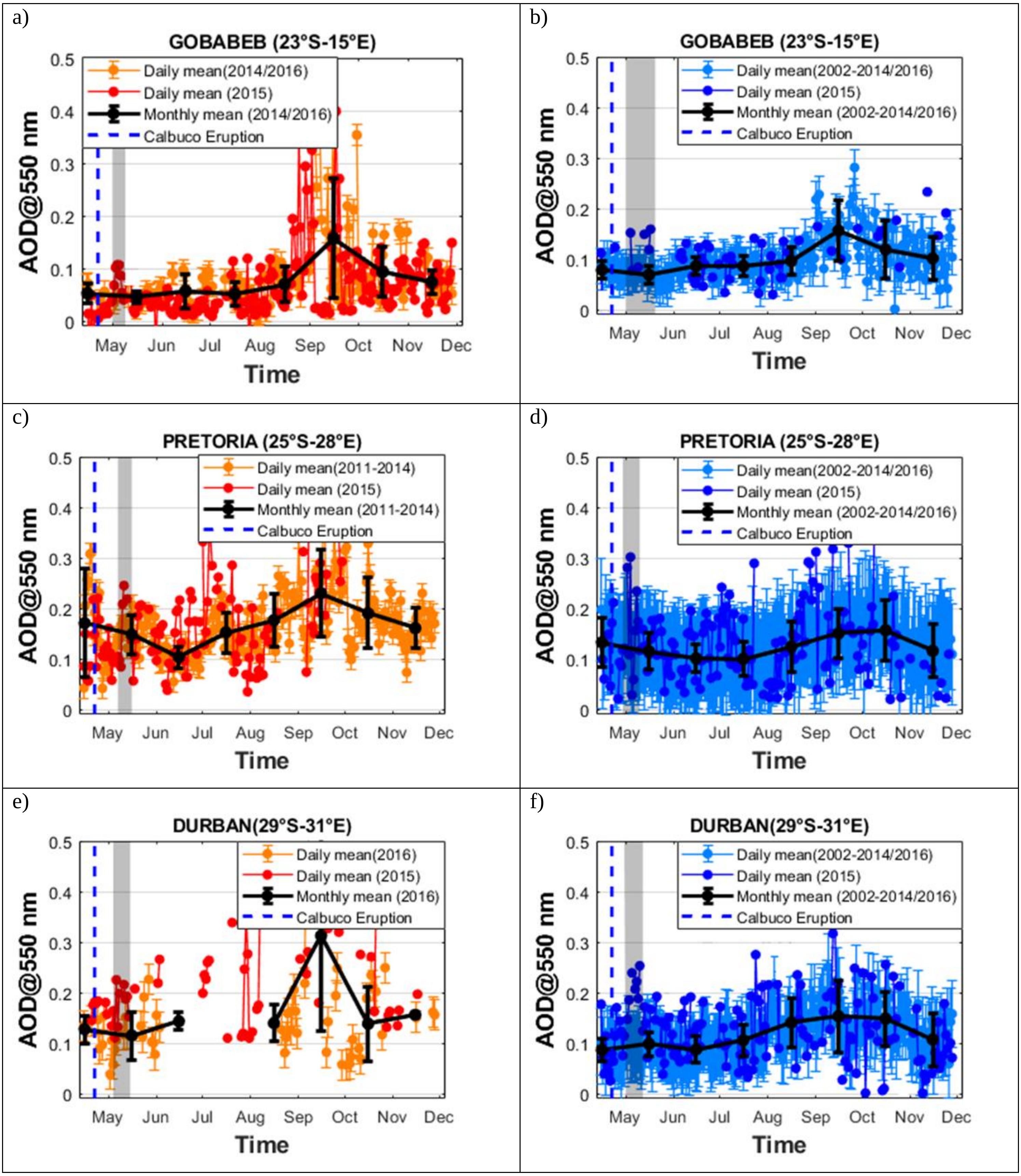

Figure 6: Daily mean of AOD (550 nm) obtained over (a,b) Gobabeb, (c,d) Pretoria and (e,f) Durban obtained from Sunphotometer (on the left panel) and from MODIS observations (on

the right panel) from 15 April to 1 December. The grey area corresponds to the influence of the volcanic plume over a given site. The black line indicates the monthly mean values.

a) Sunphotometer @ Sao Paulo

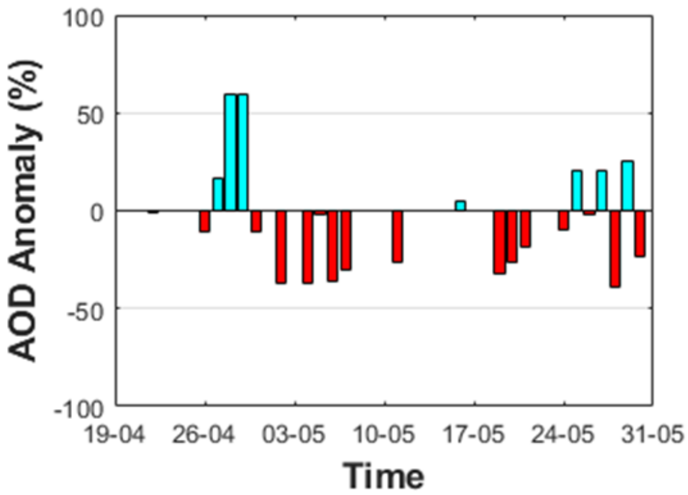

b) MODIS over Sao Paulo

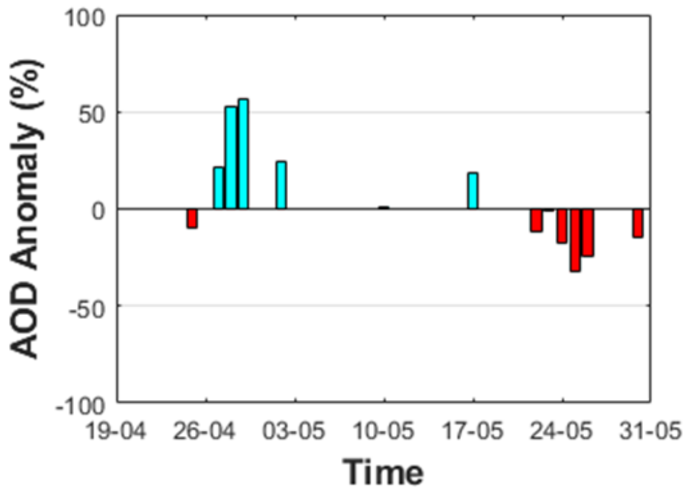

c) Sunphotometer @ Bariloche

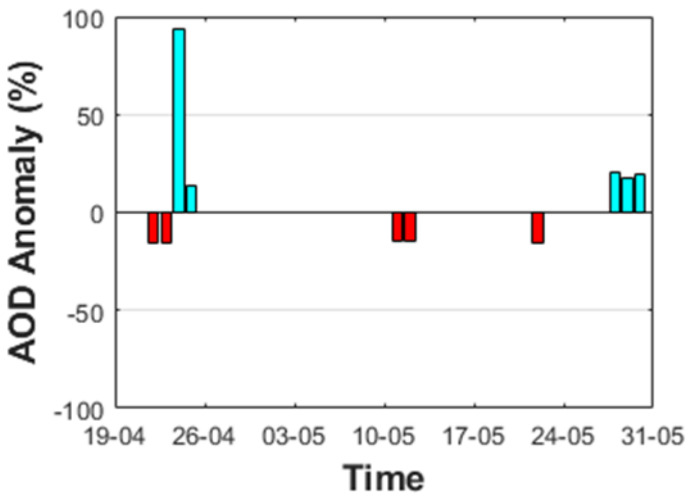

d) MODIS over Bariloche

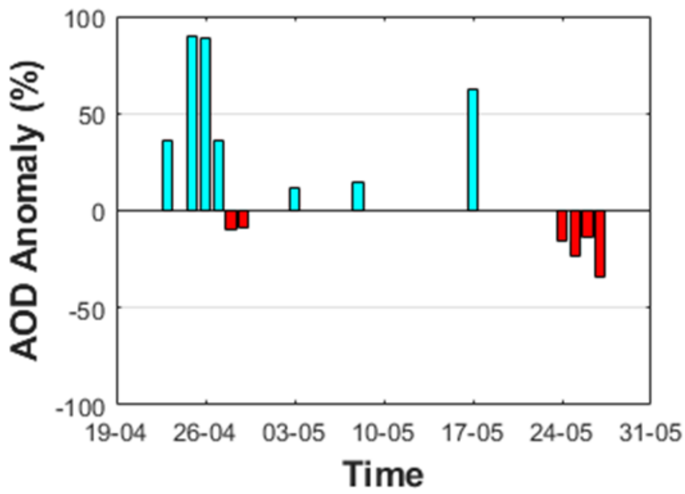

e) Sunphotometer @ Gobabeb

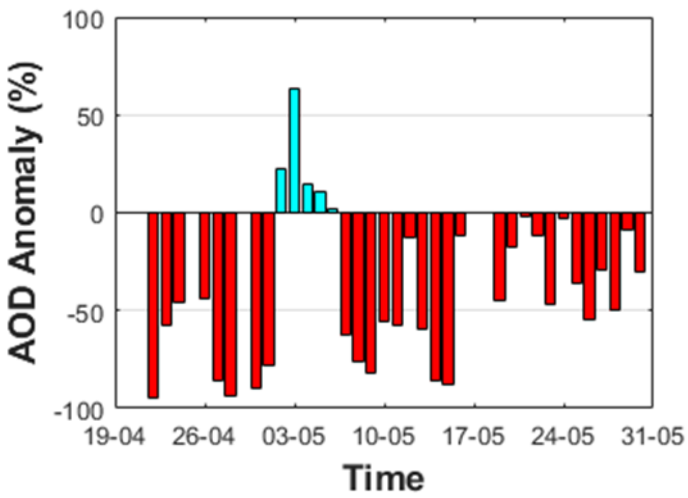

f) MODIS over Gobabeb

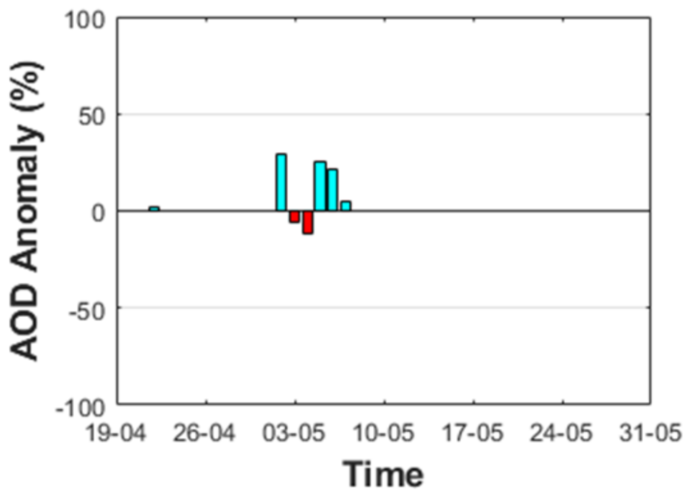

Figure 7: Daily mean of AOD anomaly (%) at (a,b) Sao Paulo, (c,d) Bariloche and (e,f) Gobabeb calculated from Sunphotometer (left panel) and MODIS (right panel) observations between 19 April and 31 May.

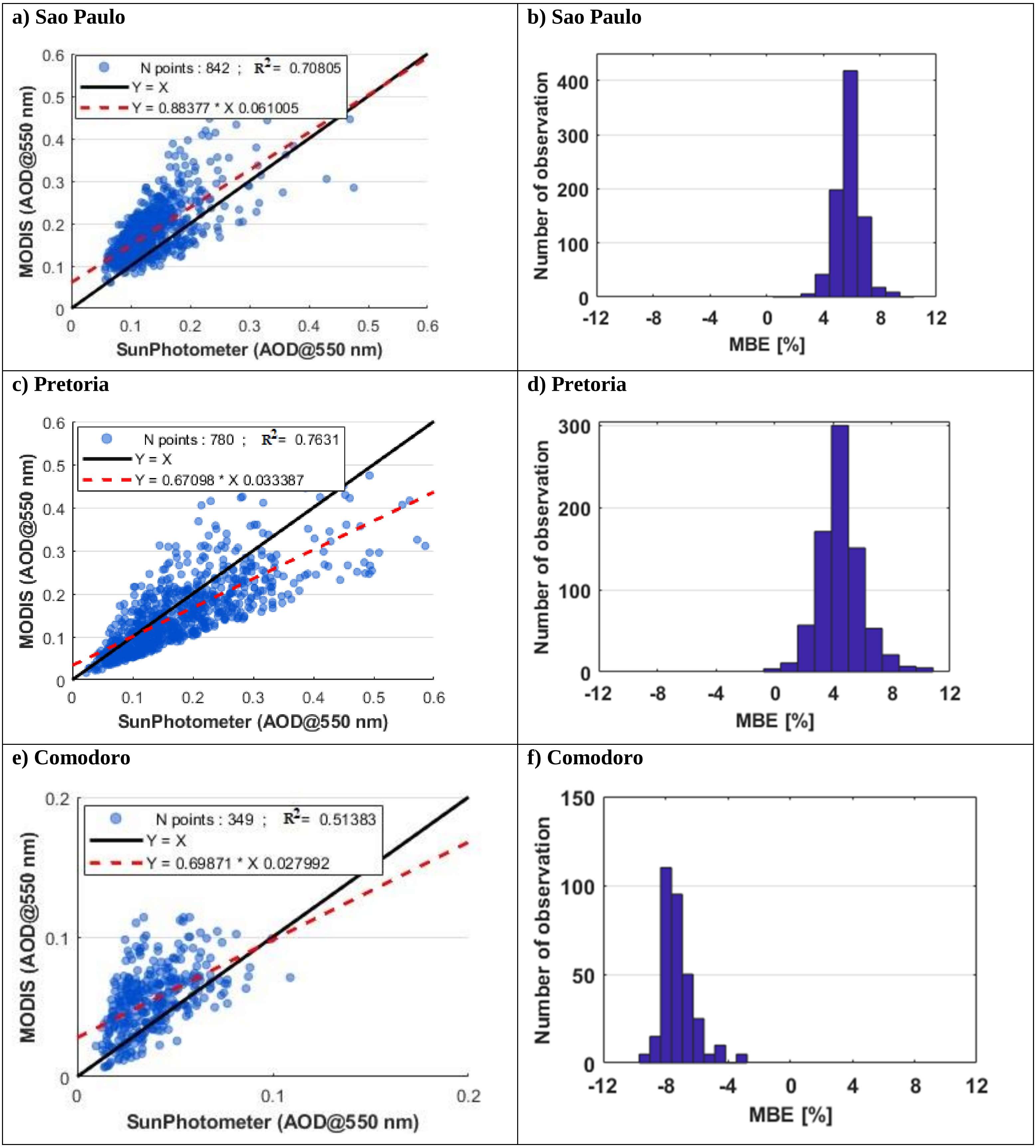

Figure 8: Correlation of AOD daily mean observations (@550 nm) between Sunphotometer and MODIS during all the period of available data at (a,b) Sao Paulo; (c,d) Pretoria and (e,f)

Comodoro. The histograms shows the mean bias error (MBE) between the two datasets by the number of observations for each site.

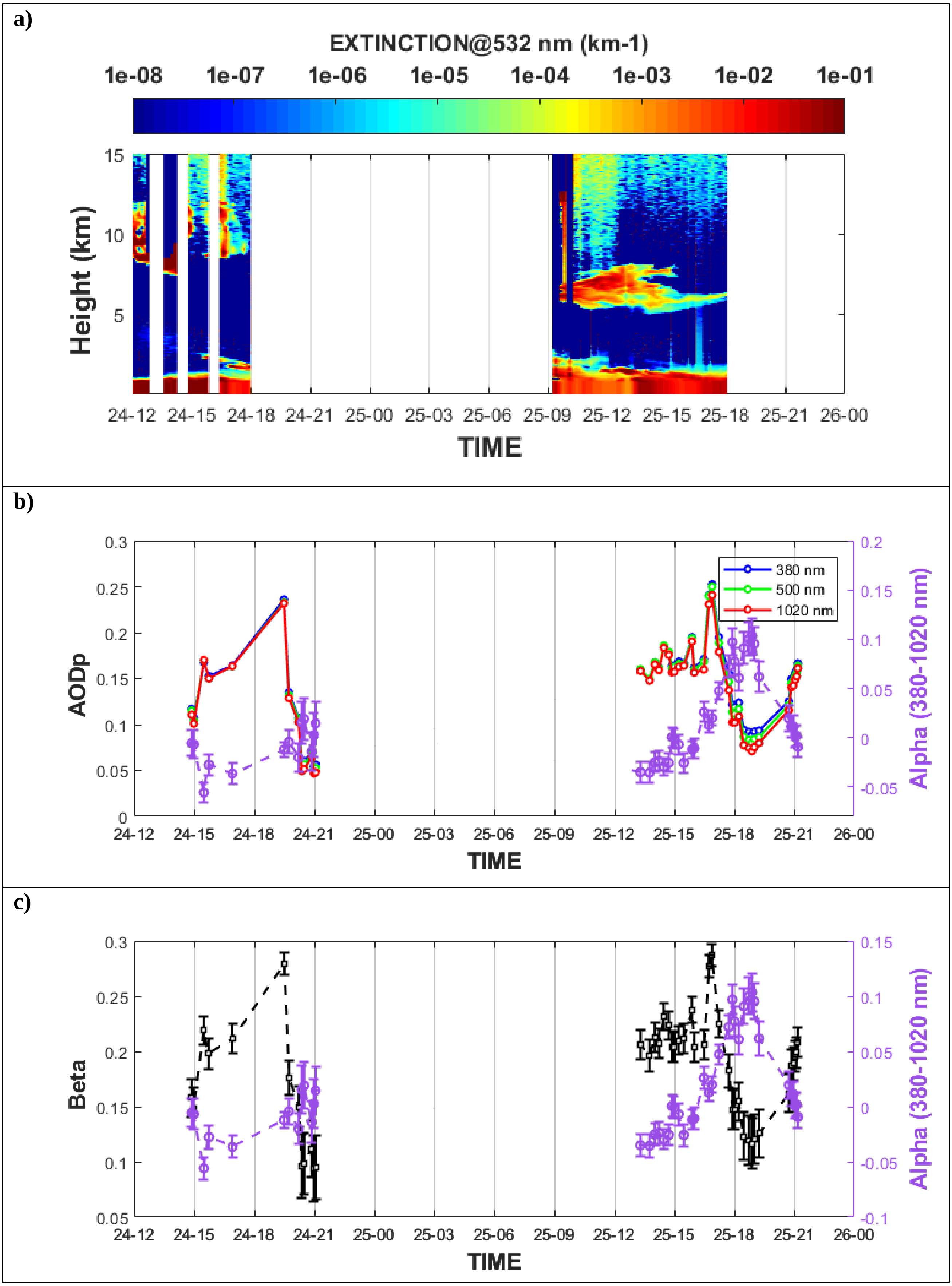

a)
EXTINCTION@532 nm (km-1)
1e-08
1e-07
1e-06
1e-05
1e-04
1e-03
1e-02
1e-01
Height (km)
15
10
5
24-12
24-15
24-18
24-21
25-00
25-03
25-06
25-09
25-12
25-15
25-18
25-21
26-00
TIME
b)
AODp
0.3
0.25
0.2
0.15
0.1
0.05
0
380 nm
500 nm
1020 nm
Alpha (380-1020 nm)
0.2
0.15
0.1
0.05
0
-0.05
24-12
24-15
24-18
24-21
25-00
25-03
25-06
25-09
25-12
25-15
25-18
25-21
26-00
TIME
c)
Beta
0.3
0.25
0.2
0.15
0.1
0.05
Alpha (380-1020 nm)
0.15
0.1
0.05
0
-0.05
-0.1
24-12
24-15
24-18
24-21
25-00
25-03
25-06
25-09
25-12
25-15
25-18
25-21
26-00
TIME

Figure 9: (a) Time evolution of the extinction profile (@532 nm) obtained from LiDAR observations at Bariloche between 24 and 25 April 2015. (b) Time evolution of the plume-isolated AOD from UV to NIR versus the Angström exponent (380-1020 nm) from Sunphotometer observations at Bariloche between 24 and 25 April 2015. (c) Time evolution of the Angström turbidity versus the Angström exponent (380-1020 nm) from Sunphotometer observations at Bariloche between 24 and 25 April 2015.

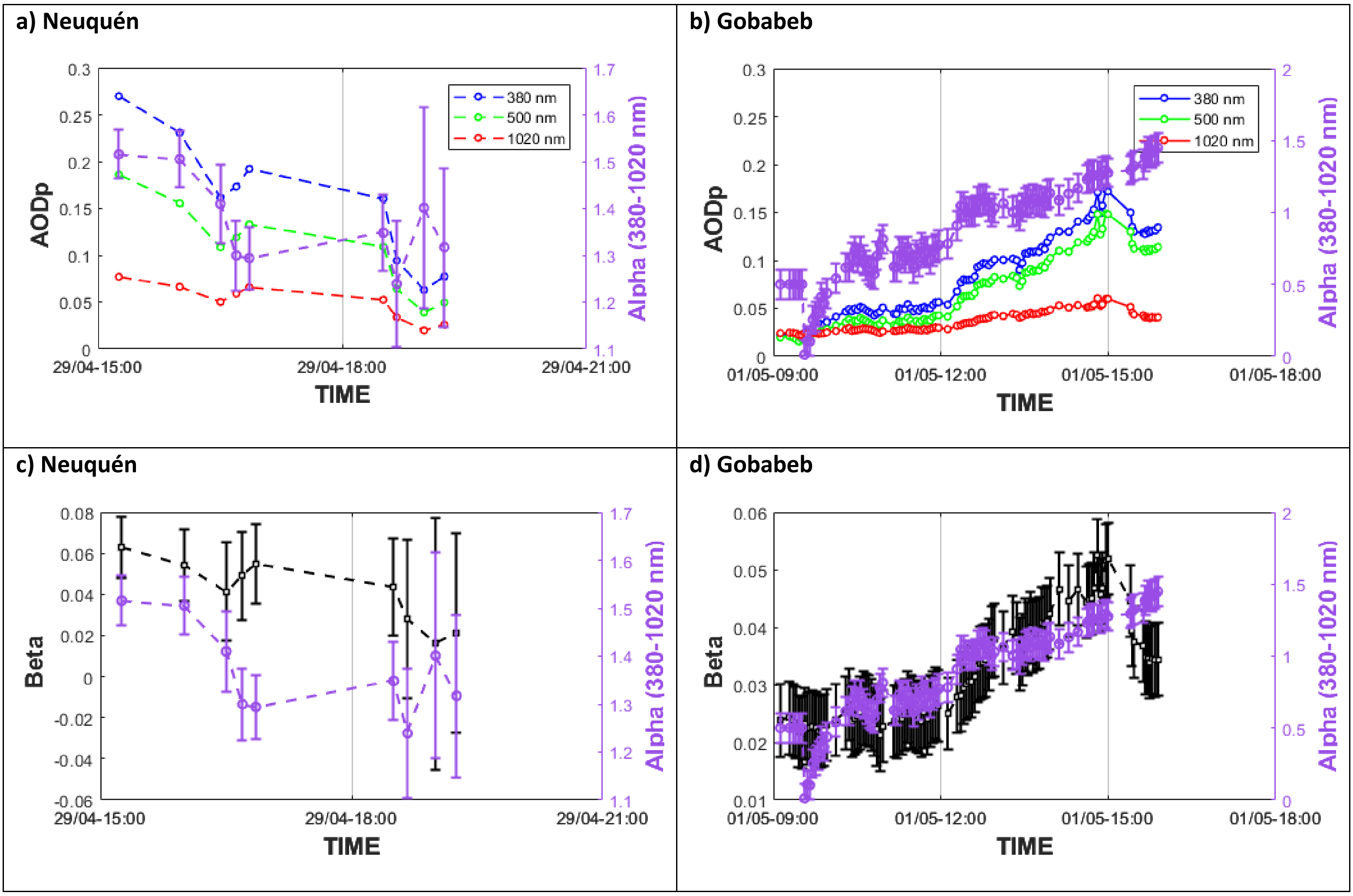

Figure 10: Time evolution of the plume-isolated AOD from UV to NIR versus Angström exponent (380-1020 nm) (a) for 29 April over Neuquén and (b) for 1 May over Gobabeb. Time evolution of Angström turbidity versus Angström exponent (380-1020 nm) (c) for 29 April over Neuquen and (d) for 1 May over Gobabeb.